iScience

CellPress
OPEN ACCESS

Article

The ApiAP2 factor PfAP2-HC is an integral component of heterochromatin in the malaria parasite *Plasmodium falciparum*

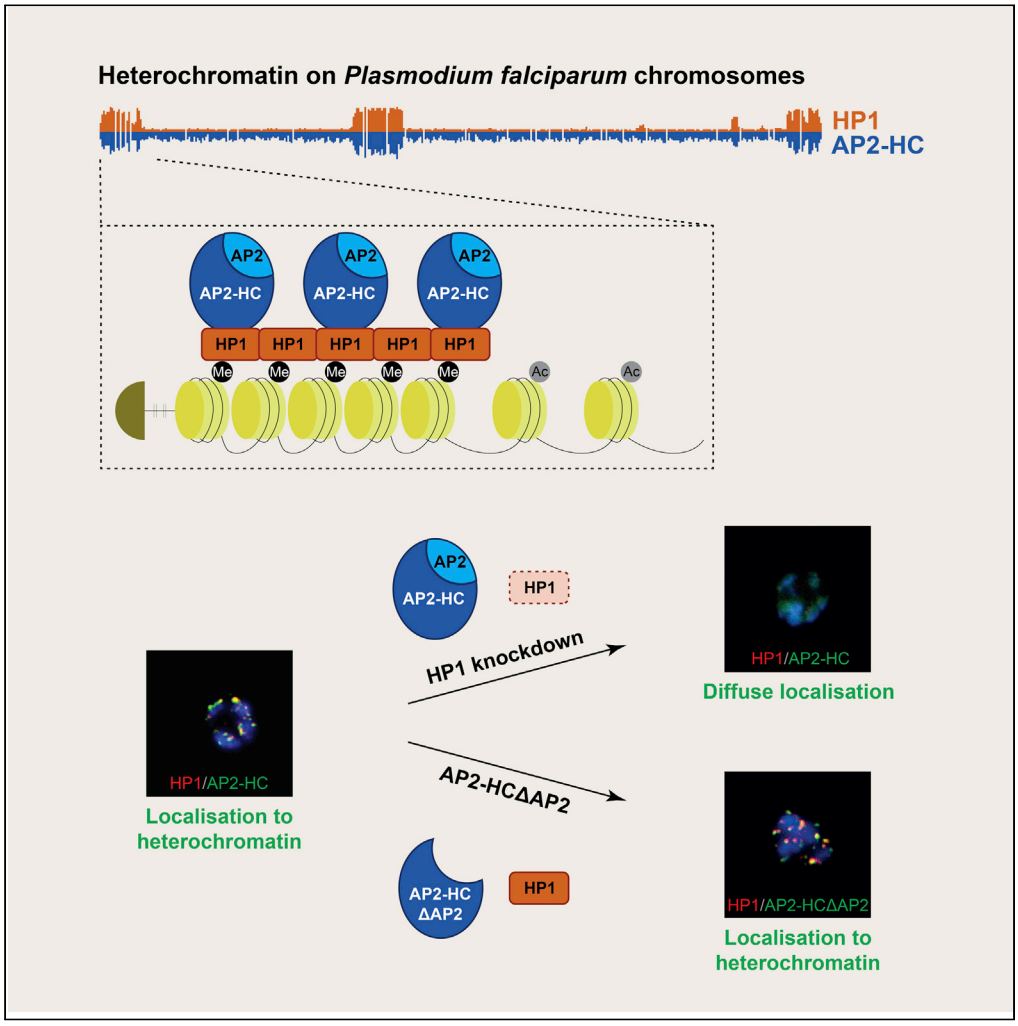

Eilidh Carrington, Roel Henrikus Martinus Cooijmans, Dominique Keller, Christa Geeke Toenhake, Richárd Bártfai, Till Steffen Voss

till.voss@swisstph.ch

Highlights

The ApiAP2 factor AP2-HC is a core component of heterochromatin in malaria parasites

Binding of AP2-HC to heterochromatin strictly depends on heterochromatin protein 1

The AP2 DNA-binding domain of AP2-HC is dispensable for heterochromatin association

Carrington et al., iScience *24*, 102444
May 21, 2021
https://doi.org/10.1016/j.isci.2021.102444

iScience

CellPress
OPEN ACCESS

Article

The ApiAP2 factor PfAP2-HC is an integral component of heterochromatin in the malaria parasite *Plasmodium falciparum*

Eilidh Carrington,[1,2] Roel Henrikus Martinus Cooijmans,[3] Dominique Keller,[1,2] Christa Geeke Toenhake,[3] Richárd Bártfai,[3] and Till Steffen Voss[1,2,4,*]

SUMMARY

Malaria parasites undergo a complex life cycle in the human host and the mosquito vector. The ApiAP2 family of DNA-binding proteins plays a dominant role in parasite development and life cycle progression. Most ApiAP2 factors studied to date act as transcription factors regulating stage-specific gene expression. Here, we characterized an ApiAP2 factor in *Plasmodium falciparum* that we termed PfAP2-HC. We demonstrate that PfAP2-HC specifically binds to heterochromatin throughout the genome. Intriguingly, PfAP2-HC does not bind DNA *in vivo* and recruitment of PfAP2-HC to heterochromatin is independent of its DNA-binding domain but strictly dependent on heterochromatin protein 1. Furthermore, our results suggest that PfAP2-HC functions neither in the regulation of gene expression nor in heterochromatin formation or maintenance. In summary, our findings reveal PfAP2-HC as a core component of heterochromatin in malaria parasites and identify unexpected properties and substantial functional divergence among the members of the ApiAP2 family of regulatory proteins.

INTRODUCTION

The apicomplexan parasite *Plasmodium falciparum* is the main cause of severe malaria worldwide, with the majority of the estimated 405,000 malarial deaths in 2018 attributed to this pathogen (WHO, 2019). The symptoms of the disease occur owing to repeated asexual intraerythrocytic developmental cycles (IDCs), where merozoite stage parasites invade human red blood cells (RBCs) and develop through the ring stage (0–24 h post invasion [hpi]) and trophozoite stage (24–30 hpi), before undergoing schizogony to produce mature segmented schizonts containing up to 32 merozoites (30–48 hpi). Rupture of the infected RBCs (iRBCs) releases the merozoites, which in turn undergo another IDC after invading new RBCs. A small proportion of schizonts per cycle commit to the sexual development pathway and produce ring stage daughter cells that mature over a period of 10 days and through four intermediate stages (I–IV) into mature stage V gametocytes (Venugopal et al., 2020). Circulating stage V gametocytes are the only forms of the parasite able to infect the mosquito vector and are therefore essential for malaria transmission.

A key trait of *P. falciparum* is the ability to adapt to and evade the constantly changing environment in its human host through clonally variant gene expression, a process vital to a broad range of biological processes, including antigenic variation, RBC invasion, solute transport, and sexual conversion (Duraisingh and Skillman, 2018; Llora-Batlle et al., 2019; Rovira-Graells et al., 2012). Clonally variant gene expression in *P. falciparum* is regulated epigenetically, with heritable gene silencing mediated by heterochromatin (Voss et al., 2014). Heterochromatin is found at subtelomeric regions on all 14 chromosomes and in some chromosome internal islands and is characterized by the binding of heterochromatin protein 1 (PfHP1) to the histone modification histone 3 lysine 9 trimethylation (H3K9me3) (Flueck et al., 2009; Fraschka et al., 2018; Lopez-Rubio et al., 2009; Perez-Toledo et al., 2009; Salcedo-Amaya et al., 2009). These PfHP1/H3K9me3-demarcated heterochromatic domains cover over 400 genes in total (approximately 8% of all protein-coding genes in the genome) (Flueck et al., 2009; Fraschka et al., 2018). As a core component of heterochromatin, PfHP1 plays an essential role in heterochromatic gene silencing and has a multi-faceted role in parasite biology as previously demonstrated with a conditional loss-of-function mutant (Brancucci et al., 2014). Conditional depletion of PfHP1 resulted in the de-repression of multi-copy gene families important in antigenic variation, including the well-characterized *var* gene family (Brancucci et al., 2014; Scherf

[1]Department of Medical Parasitology and Infection Biology, Swiss Tropical and Public Health Institute, 4051 Basel, Switzerland

[2]University of Basel, 4001 Basel, Switzerland

[3]Department of Molecular Biology, Radboud University, 6525GA Nijmegen, The Netherlands

[4]Lead contact

*Correspondence: till.voss@swisstph.ch

https://doi.org/10.1016/j.isci.2021.102444

et al., 2008). In addition, around half of progeny parasites depleted of PfHP1 underwent gametocytogenesis due to de-repression of the internal heterochromatic *pfap2-g* locus encoding the master transcriptional regulator of gametocytogenesis, PfAP2-G (Brancucci et al., 2014; Kafsack et al., 2014; Sinha et al., 2014). The remaining progeny arrested at the trophozoite stage, indicating an essential role of PfHP1 in proliferation (Brancucci et al., 2014). With such a diverse range of processes reliant on PfHP1 and heterochromatic gene silencing, the mechanisms of this system warrant further study. However, the molecular machinery involved in heterochromatin establishment, spreading, and maintenance in *P. falciparum* remain elusive, along with the transcription factors involved in regulating the expression of heterochromatic genes.

The main transcription factor family in Apicomplexan parasites is the ApiAP2 group of DNA-binding proteins, comprising 27 members in *P. falciparum* (Balaji et al., 2005; Jeninga et al., 2019; Painter et al., 2011). ApiAP2 proteins are characterized by the presence of one to three AP2 domains, homologous to the DNA-binding domains of plant APETALA2/ethylene response element binding protein (AP2/EREBP) transcription factors (Balaji et al., 2005; Dietz et al., 2010). To date, five members have been functionally analyzed in *P. falciparum*, three of which are acting as transcription factors. PfAP2-G, as mentioned above, is the master regulator of sexual commitment (Kafsack et al., 2014) and has recently been confirmed as an activator of gametocyte genes, with an additional role in regulating RBC invasion genes suggested (Josling et al., 2020). PfAP2-I is likely essential for parasite survival and regulates a subset of gene families involved in RBC invasion (Santos et al., 2017). Of interest, PfAP2-I and PfAP2-G also bind upstream of several genes encoding ApiAP2 factors, which could suggest a complex regulatory interplay between ApiAP2 family members (Josling et al., 2020; Santos et al., 2017). Indeed, Josling and colleagues provided evidence of cooperative binding of PfAP2-G and PfAP2-I to some invasion gene promoters (Josling et al., 2020). PfAP2-EXP is involved in regulating multi-gene families, including *rif*, *stevor*, and *pfmc-2tm*, and is seemingly essential for asexual growth (Martins et al., 2017). In contrast, PfSIP2 predominantly binds to SPE2 motifs found in telomere-associated repeat elements (TAREs) and upstream of subtelomeric upsB *var* genes, both of which are heterochromatic, suggesting a possible role in heterochromatin and/or chromosome end biology (Flueck et al., 2010). Finally, PfAP2-Tel binds to telomere repeats on all 14 chromosomes and is likely involved in telomere maintenance mechanisms (Sierra-Miranda et al., 2017). Beyond these studies in *P. falciparum*, much has been achieved in characterizing ApiAP2 proteins of *Plasmodium* species infecting rodents. In *P. berghei*, several ApiAP2 factors with essential roles in gametocytogenesis (Sinha et al., 2014; Yuda et al., 2015, 2020) and in the mosquito and liver stages (Iwanaga et al., 2012; Kaneko et al., 2015; Yuda et al., 2009, 2010) have been studied. In addition, systematic knockout screens in *P. berghei* (Modrzynska et al., 2017) and *P. yoelii* (Zhang et al., 2017) provided an extensive characterization of the ApiAP2 family and highlight essentiality at different life cycle stages. Of interest, although some orthologs have the same function in *P. falciparum* and *P. berghei*, for example, AP2-G (Kafsack et al., 2014; Sinha et al., 2014), others display differences such as the PfAP2-EXP ortholog PbAP2-SP, which is expressed exclusively in the sporozoite stages of *P. berghei* (Yuda et al., 2010).

We recently identified the ApiAP2 protein PF3D7_1456000 as a putative interaction partner of PfHP1 using co-immunoprecipitation (coIP) experiments coupled with protein mass spectrometry (Filarsky et al., 2018). Here, we present a multifaceted approach to dissect the potential functions of this ApiAP2 factor in heterochromatin-associated processes during blood stage development of *P. falciparum* parasites.

RESULTS

PfAP2-HC specifically associates with heterochromatin

We recently identified a list of potential PfHP1 interaction partners, which includes a member of the ApiAP2 family of putative transcription factors, PF3D7_1456000 (Filarsky et al., 2018), hereafter referred to as PfAP2-HC. To validate the interaction between PfAP2-HC and PfHP1, we employed a two-plasmid CRISPR-Cas9-based gene editing approach to N-terminally tag PfAP2-HC with GFP (GFP-PfAP2-HC) (Figures 1A and S1). We tagged the N terminus because the single AP2 domain of PfAP2-HC is located right at the C terminus of the protein where tagging may interfere with its function. We obtained a clonal line of the resulting 3D7/GFP-PfAP2-HC population by limiting dilution cloning and confirmed correct editing of the locus by PCR on genomic DNA (gDNA) (Figure S1). Live cell fluorescence imaging of GFP-PfAP2-HC revealed a perinuclear localization, which was undetectable in ring stages and first appeared in trophozoites, peaking mid-schizogony and decreasing in late schizonts (Figure S1). This temporal expression pattern is consistent with the transcriptional profile of *pfap2-hc* during the IDC (Bartfai et al., 2010). The localization pattern of

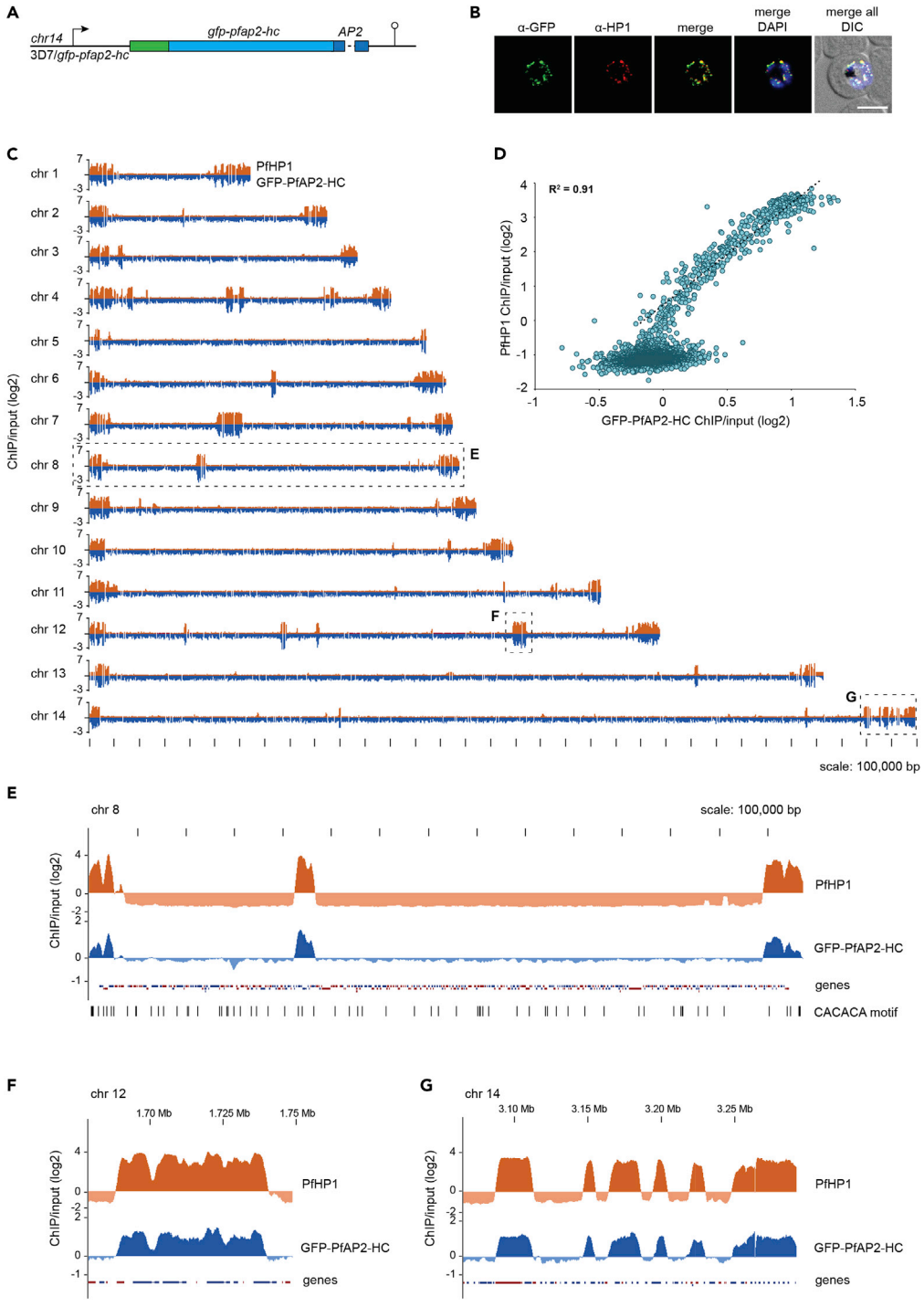

Figure 1. PfAP2-HC associates with PfHP1 throughout the genome

(A) Schematic map of the endogenous *pfap2-hc* locus after introduction of a *gfp* tag by CRISPR-Cas9-mediated gene editing in 3D7/GFP-PfAP2-HC parasites. See also Figure S1.

(B) Representative IFA images of GFP-PfAP2-HC and PfHP1 localization in 3D7/GFP-PfAP2-HC parasites, 36–44 hpi. Nuclei were stained with DAPI. DIC, differential interference contrast. Scale bar, 5 μm.

(C) Log2-transformed α-PfHP1 (orange) and α-GFP (blue) ChIP-over-input ratio tracks obtained from 3D7/GFP-PfAP2-HC schizont stage parasites. α-PfHP1 and α-GFP ChIP tracks have been offset by 2 and 1, respectively, to be able to display the full scale of variation. In addition, α-GFP ChIP-seq data are mirrored on a negative scale. Dashed boxes highlight regions that are enlarged in (E)–(G).

Figure 1. *Continued*

(D) Scatterplot of average log2-transformed α-PfHP1 and α-GFP ChIP-over-input values for all parasite genes. The depicted regression line is based on heterochromatic genes only (log2 ratio α-PfHP1/input ≥0). The coefficient of determination (R^2) is displayed in the upper left corner. See also Data S1.

(E) Log2-transformed ChIP-over-input ratio tracks on chromosome 8. The locations of the putative PfAP2-HC binding motif (CACACA) (Campbell et al., 2010) are shown below the tracks (FDR <0.05). Coding sequences are shown as blue (sense strand) and red (antisense strand) boxes.

(F and G) Log2-transformed ChIP-over-input ratio tracks over sections of chromosome 12 and 14, respectively.

GFP-PfAP2-HC matches that of PfHP1 in immunofluorescence assays (IFAs), where the two proteins appear to overlap (Figure 1B).

In order to investigate the genome-wide binding profile of GFP-PfAP2-HC and to allow comparison with PfHP1 at high resolution, we performed chromatin immunoprecipitation-sequencing (ChIP-seq) using α-GFP and α-PfHP1 antibodies to compare binding profiles within the same parasite population. We found that GFP-PfAP2-HC indeed co-localizes with PfHP1 throughout the genome (Figures 1C, 1E, 1F and 1G). To quantify the degree of co-localization, we computed and compared PfHP1 and PfAP2-HC ChIP-over-input enrichment values in coding regions across the genome (Data S1). This confirmed a strong correlation (R^2 = 0.91) between PfAP2-HC and PfHP1 occupancies across coding regions of all heterochromatic genes (Figure 1D). In addition, we visualized on all chromosomes the locations of the putative PfAP2-HC target DNA motif (CACACA) as predicted by *in vitro* binding preference of the recombinant PfAP2-HC AP2 DBD (Campbell et al., 2010). The CACACA motif showed no enrichment in heterochromatic over euchromatic regions and therefore showed no positional association with the *in vivo* PfAP2-HC binding profile (Figure 1E). Collectively, these findings show that PfAP2-HC localizes exclusively to PfHP1-defined heterochromatic regions and seems not to bind to the predicted CACACA target motifs *in vivo*.

PfAP2-HC is not required for heterochromatin maintenance and inheritance

Having shown that PfAP2-HC shares the genome-wide binding profile of PfHP1, we next investigated the function of this ApiAP2 factor by creating a conditional knockdown line employing the FKBP destabilization domain (DD) system. DD-tagged proteins are stabilized in the presence of the small molecule Shield-1, and removal of this ligand leads to protein degradation (Armstrong and Goldberg, 2007; Banaszynski et al., 2006). We utilized our two-plasmid CRISPR-Cas9 approach to N-terminally tag PfAP2-HC with DDGFP to create the cell line 3D7/DDGFP-PfAP2-HC (Figures 2A and S2). Limiting dilution cloning resulted in a parasite clone containing the correctly edited locus, which we confirmed by PCR on gDNA (Figure S2). Substantial depletion of DDGFP-PfAP2-HC expression in the absence of Shield-1 was verified by live cell fluorescence imaging (Figure 2B) and Western blot (Figures 2C and S2). Depletion of DDGFP-PfAP2-HC expression caused no major cell cycle- or proliferation-related phenotypes nor did it have an effect on sexual conversion rates (Figure S3).

In order to investigate the potential effect of PfAP2-HC depletion on heterochromatin, we grew parasites in the presence or absence of Shield-1 for 13 generations and compared their genome-wide PfHP1 binding profiles by ChIP-seq. The genome-wide PfHP1 coverage tracks in 3D7/DDGFP-PfAP2-HC parasites grown in the absence or presence of Shield-1 are highly similar (Figure 2D). Likewise, the genome-wide PfHP1 coverage of coding regions in the two populations is nearly identical (R^2 = 0.99) (Figure 2E and Data S1) showing that depletion of PfAP2-HC has no discernible effect on PfHP1 localization on chromatin. To test whether the lack of obvious loss-of-function phenotypes was due to the residual amounts of DDGFP-PfAP2-HC protein remaining after Shield-1 removal (Figure 2C), we also generated a PfAP2-HC knockout cell line, 3D7/PfAP2-HC-KO (Figure S4), which we confirmed by PCR on gDNA (Figure S4). 3D7/PfAP2-HC-KO parasites did not show obvious growth-related phenotypic changes either (Figure S4) and maintained PfHP1 occupancy at levels similar to 3D7 wildtype (3D7/WT) and 3D7/DDGFP-PfAP2-HC parasites (Figure 2D). Changes in PfHP1 coverage of some genes were observed in 3D7/PfAP2-HC-KO parasites compared with 3D7/WT and 3D7/DDGFP-PfAP2-HC (Figures 2F and S4 and Data S1). However, these changes are likely unrelated to the lack of PfAP2-HC expression but rather attributable to clonally variant changes in PfHP1 occupancy as similar differences are observed when comparing different PfAP2-HC-expressing clonal lines (3D7/WT and 3D7/DDGFP-PfAP2-HC) (Figure S4). Together, these results show that PfAP2-HC is neither required for asexual proliferation nor for the maintenance and inheritance of PfHP1-demarcated heterochromatin.

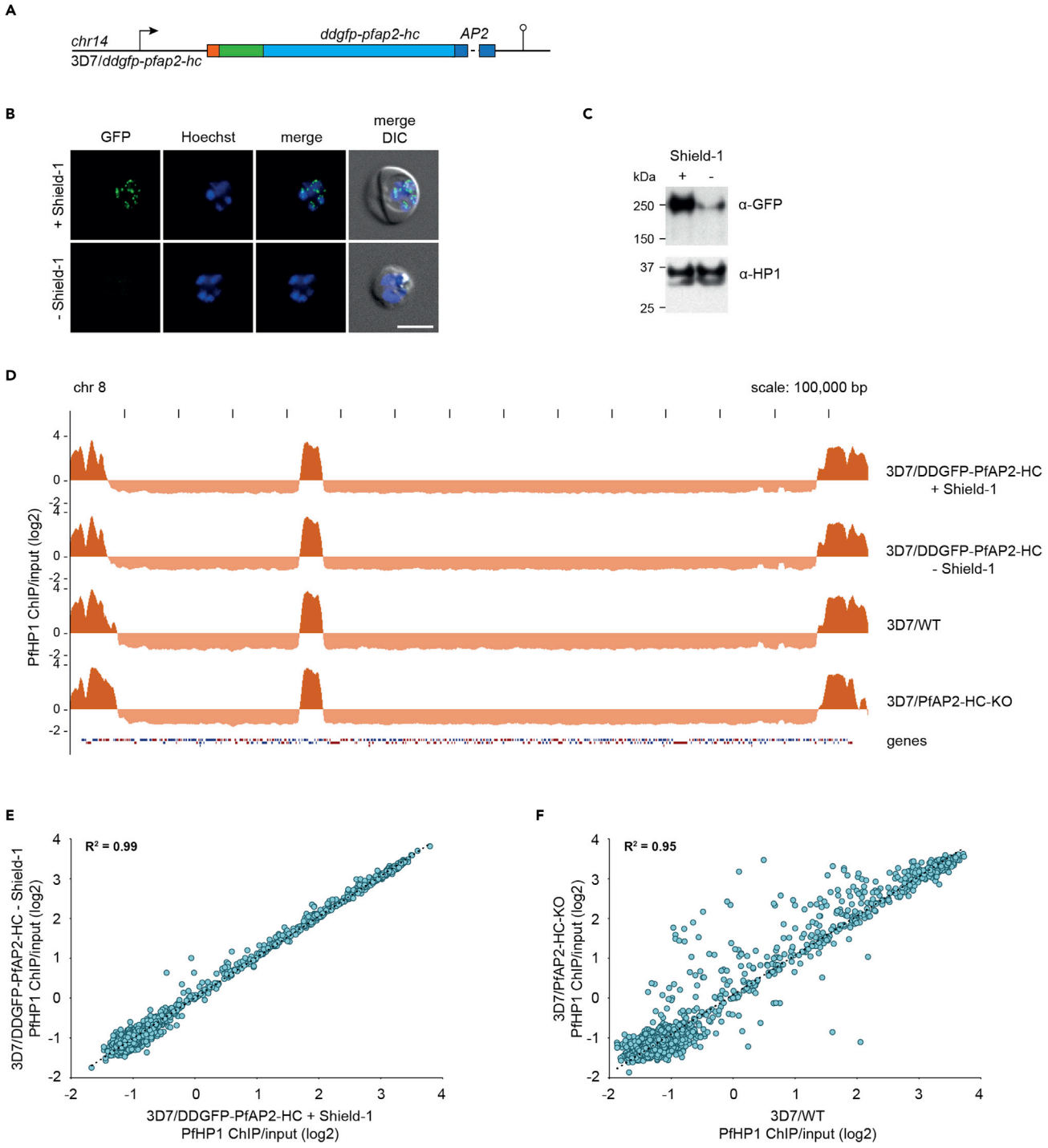

Figure 2. PfAP2-HC depletion does not affect PfHP1 genome-wide coverage

(A) Schematic map of the endogenous *pfap2-hc* locus after CRISPR-Cas9-mediated gene editing to introduce *ddgfp* tag in 3D7/DDGFP-PfAP2-HC parasites. See also Figure S2.

(B) Representative live cell fluorescence images of 3D7/DDGFP-PfAP2-HC schizonts (36–44 hpi) grown in the presence (+) or absence (–) of Shield-1. Nuclei were stained with Hoechst. DIC, differential interference contrast. Scale bar, 5 μm. See also Figure S3.

(C) Western blot showing DDGFP-PfAP2-HC expression levels in 3D7/DDGFP-PfAP2-HC schizonts (36–44 hpi) grown in the presence (+) or absence (–) of Shield-1. PfHP1 expression levels served as a loading control. The full-sized blot is available in Figure S2.

Figure 2. *Continued*

(D) Log2-transformed α-PfHP1 ChIP-over-input tracks from 3D7/DDGFP-PfAP2-HC schizont stage parasites grown in the presence (+) or absence (–) of Shield-1 (top two tracks). Log2-transformed α-PfHP1 ChIP-over-input tracks from 3D7/WT and 3D7/PfAP2-HC-KO schizonts (bottom two tracks). Coding sequences are shown as blue (sense strand) and red (antisense strand) boxes. See also Figure S4.

(E and F) Scatterplots of average log2-transformed α-PfHP1 ChIP-over-input values at all coding regions in 3D7/DDGFP-PfAP2-HC schizonts grown in the presence (+) or absence (–) of Shield-1 (E) and in 3D7/WT and 3D7/PfAP2-HC-KO schizonts (F). Depicted regression lines are based on heterochromatic genes only (log2 ratio α-PfHP1/input ≥0). The coefficient of determination (R^2) is shown in the upper left corner. See also Data S1.

PfAP2-HC does not act as a transcription factor in blood stage parasites

To identify any possible role of PfAP2-HC in transcriptional regulation we performed a transcriptome-wide microarray time course analysis. We compared 3D7/DDGFP-PfAP2-HC parasites grown in the presence and absence of Shield-1 across five time points throughout the IDC (Figure 3A). For each of the five time points the paired transcriptome data were strongly correlated based on Pearson correlation values, demonstrating highly comparable stage composition across the time course (Figure 3A and Data S2). We found no significant difference in gene expression, with no transcripts showing greater than 2-fold average fold change in steady-state mRNA abundance between the +Shield-1 and -Shield-1 populations (Figure 3B), suggesting that PfAP2-HC does not play a dominant role in transcriptional regulation in blood stage parasites and further corroborating the lack of obvious phenotypes associated with PfAP2-HC depletion.

The AP2 domain of PfAP2-HC is dispensable for targeting PfAP2-HC to heterochromatin

To discern the importance of the single AP2 DBD in targeting PfAP2-HC to heterochromatin we introduced a STOP codon prior to the AP2 domain, replacing amino acid R1319 with a premature STOP codon in 3D7/GFP-PfAP2-HC to create the parasite line 3D7/GFP-PfAP2-HC-ΔDBD (Figures 4A and S5). PCR on gDNA confirmed successful editing of the locus (Figure S5). The transgenic population consisted of a mixture of parasites either with correctly edited locus or carrying integrated donor plasmid concatemers (Figure S5). Of importance, both recombination events introduce the desired premature STOP codon into the *pfap2-hc* coding sequence. Indeed, Sanger sequencing of the amplified PCR products verified successful introduction of the premature STOP codon in the entire population (Figure S5). The localization of GFP-PfAP2-HC-ΔDBD is comparable with that of GFP-PfAP2-HC by IFA and similarly shares this localization pattern with PfHP1 (Figure 4B).

For a more comprehensive analysis, we again performed ChIP-seq experiments using α-GFP and α-PfHP1 antibodies on 3D7/GFP-PfAP2-HC-ΔDBD parasites. As with full-length GFP-PfAP2-HC, the truncated PfAP2-HC-ΔDBD protein co-localized with PfHP1 throughout the genome with highly correlated enrichment on all heterochromatic genes (Figures 4C and 4D and Data S1) showing that the AP2 DBD of PfAP2-HC is dispensable for its localization to heterochromatin.

Binding of PfAP2-HC to heterochromatin is PfHP1 dependent

PfAP2-HC is targeted to heterochromatin in the absence of its only recognizable DBD, suggesting a reliance on protein-protein interactions independent of the AP2 domain. To gain insight into this interaction, we tagged PfHP1 with the fluorescent protein mScarlet. In addition, we introduced a sequence encoding the *glms* riboswitch element (Prommana et al., 2013) downstream of the STOP codon, such that the resulting *pfhp1-mscarlet* mRNA contains a functional *glms* ribozyme in its 3′ untranslated region. Upon addition of glucosamine (GlcN) to the culture medium, the *glms* ribozyme mediates mRNA cleavage and degradation (Prommana et al., 2013; Watson and Fedor, 2011). We generated this conditional PfHP1 knockdown cassette in the background of the 3D7/GFP-PfAP2-HC clone to create the 3D7/GFP-PfAP2-HC/PfHP1-mScarlet-glmS double transgenic parasite line (Figures 5A and S6). We confirmed correct editing of the *pfhp1* locus by PCR on gDNA (Figure S6). To investigate the effect of PfHP1 depletion on the localization of GFP-PfAP2-HC, we split 3D7/GFP-PfAP2-HC/PfHP1-mScarlet-glmS parasites at 0–8 hpi into two populations, adding GlcN to one of them to induce the knockdown of PfHP1-mScarlet expression (+GlcN) and keeping the other one under stabilizing conditions (-GlcN). Live cell fluorescence imaging and Western blot analysis of schizont stage parasites confirmed the efficient depletion of PfHP1-mScarlet expression in +GlcN conditions (Figures 5B, 5C, and S6). Of interest, upon PfHP1-mScarlet depletion, GFP-PfAP2-HC localized diffusely throughout the nucleoplasm and no longer displayed a punctate perinuclear pattern (Figure 5B), showing mis-localization in the absence of PfHP1.

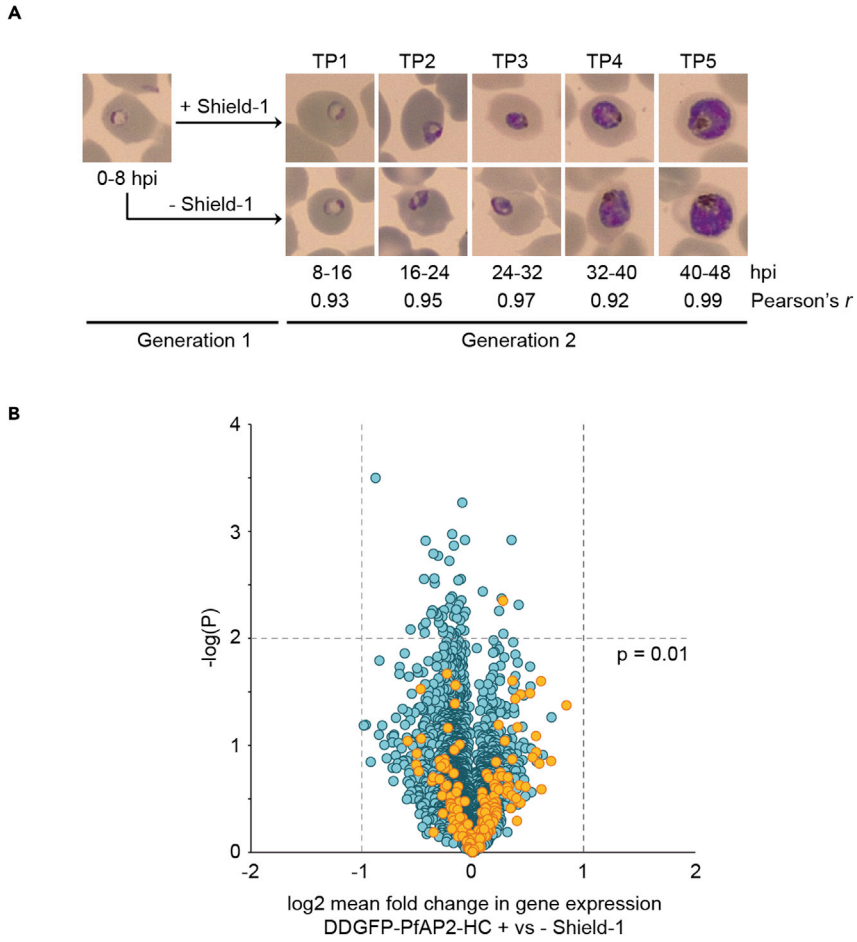

Figure 3. Depletion of PfAP2-HC has no effect on transcription in asexual blood stage parasites

(A) 3D7/DDGFP-PfAP2-HC parasites were grown in the presence (+) or absence (–) of Shield-1 from 0–8 hpi for one generation and sampled for comparative transcriptome analysis at five IDC time points in the subsequent generation. Pearson correlation coefficients *r* indicate the pairwise correlation between the paired transcriptomes of parasites cultured in the presence (+) or absence (–) of Shield-1 for each time point. TP, time point. See also Data S2.

(B) Volcano plot showing log2 fold changes in relative transcript abundance averaged across the five time points and plotted against significance [-log10(p value)]. Euchromatic and heterochromatic genes are depicted by blue and orange circles, respectively. See also Data S2.

The ChIP-seq results presented in Figure 1 provided no evidence for direct binding of PfAP2-HC to DNA in euchromatic regions. However, this experiment did not allow us to test if PfAP2-HC binds to DNA sequences in heterochromatic regions because its association with PfHP1 would have masked such interactions. Hence, we used the 3D7/GFP-PfAP2-HC/PfHP1-mScarlet-glmS line to ask whether PfAP2-HC binds directly to DNA in the absence of PfHP1. We grew 3D7/GFP-PfAP2-HC/PfHP1-mScarlet-glmS parasites in the presence of GlcN from early ring stages (0–8 hpi) and harvested samples for ChIP-seq at 40–48 hpi within the same cycle. As expected, we observed a large reduction in PfHP1 enrichment in heterochromatic domains (Figure 5D). GFP-PfAP2-HC occupancy was massively reduced, and in two biologically independent ChIP-seq experiments we could not detect signals over background (Figure 5D and Data S1). Together, these results show that PfAP2-HC localization to heterochromatin is entirely dependent on PfHP1 and no evidence for direct binding of PfAP2-HC to DNA in these regions could be discerned.

PfAP2-HC is likely not involved in heterochromatin formation

We have shown that maintenance and inheritance of heterochromatin was unaffected in both the 3D7/PfAP2-HC-KO null mutant and in the conditional 3D7/DDGFP-AP2-HC loss-of-function mutants after 13

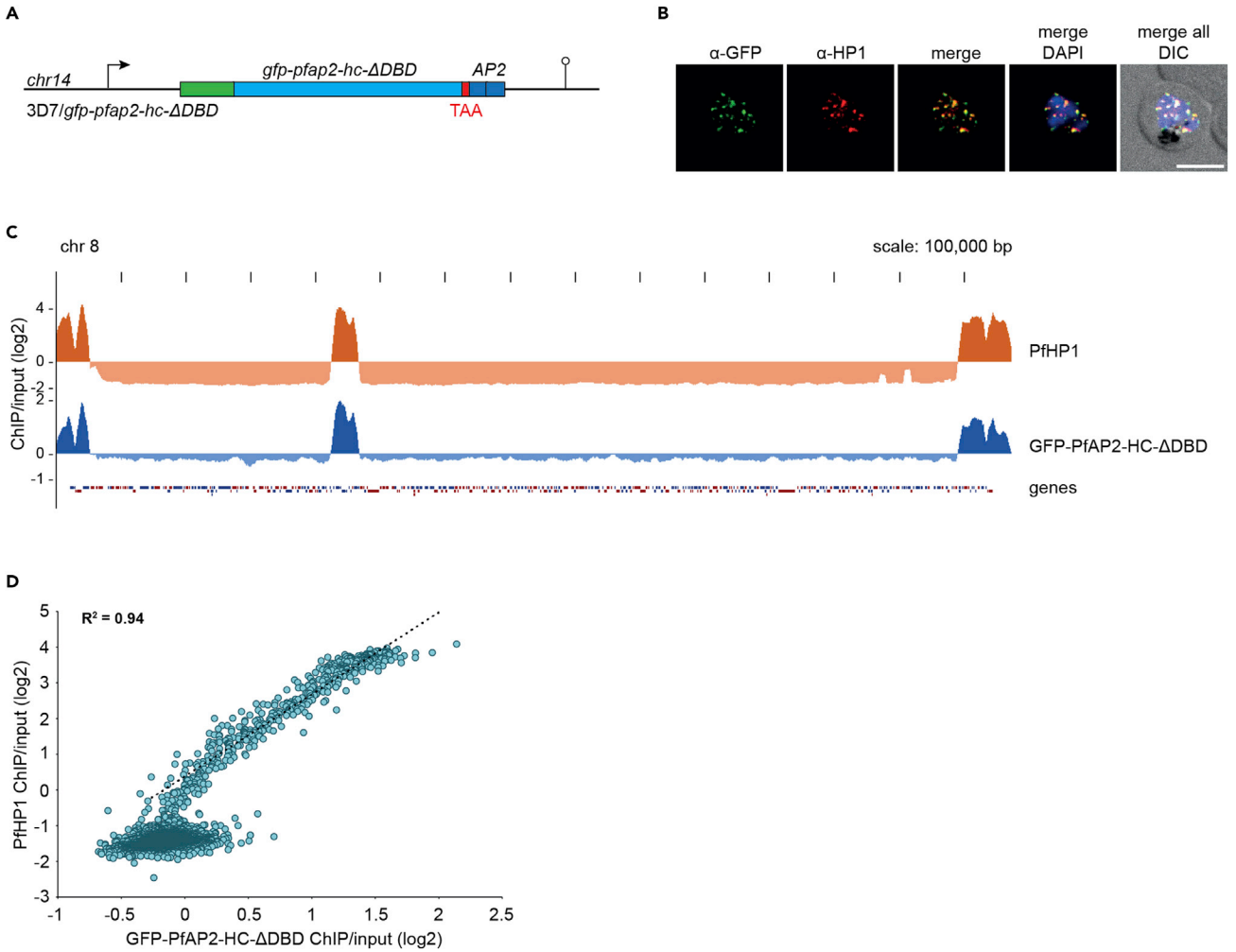

Figure 4. The AP2 domain of PfAP2-HC is not required for heterochromatin targeting

(A) Schematic map of the *gfp-pfap2-hc* locus after CRISPR-Cas9-mediated gene editing to introduce a STOP codon prior to the sequence encoding the AP2 DBD in 3D7/GFP-PfAP2-HC-ΔDBD parasites. See also Figure S5.

(B) Representative IFA images of GFP-PfAP2-HC-ΔDBD and PfHP1 localization in a developing schizont (36–44 hpi). Nuclei were stained with DAPI. DIC, differential interference contrast. Scale bar, 5 μm.

(C) Log2-transformed α-PfHP1 (orange) and α-GFP (blue) ChIP-over-input tracks from 3D7/GFP-PfAP2-HC-ΔDBD schizont stage parasites.

(D) Scatterplot of average log2-transformed α-PfHP1 and α-GFP ChIP-over-input values at all coding regions. The regression line is based on heterochromatic genes only (log2 ratio α-PfHP1/input ≥0). The coefficient of determination (R^2) is displayed in the upper left corner. See also Data S1.

generations of growth under PfAP2-HC-depleted conditions (Figure 2D). However, factors influencing the initial establishment of heterochromatin can be independent of maintenance and inheritance (Sadaie et al., 2004). Taking advantage of the fact that conditional knockdown of PfHP1 expression produces progeny consisting of approximately 50% viable heterochromatin-depleted early-stage gametocytes and 50% growth-arrested trophozoites (Brancucci et al., 2014), we investigated whether PfAP2-HC is required for the re-establishment of heterochromatin during gametocyte maturation. To achieve this, we generated a parasite line allowing for the conditional knockdown of both PfHP1 and PfAP2-HC, 3D7/DDGFP-PfAP2-HC/PfHP1-mScarlet-glmS (Figures 6A and S6). The 3D7/DDGFP-PfAP2-HC/PfHP1-mScarlet-glmS line was obtained by tagging the *pfhp1* gene in the 3D7/DDGFP-AP2-HC clone with *mscarlet-glmS* as described above (Figure S6). We confirmed correct editing of the *pfhp1* locus by PCR on gDNA (Figure S6). Routine culture of this parasite line in the presence of Shield-1 and absence of GlcN stabilizes DDGFP-PfAP2-HC and PfHP1-mScarlet expression, respectively. We divided ring stage parasites into two populations at 0–8 hpi (generation 1), of which one was maintained under stabilizing conditions for both proteins and from the other one Shield-1 was removed to induce DDGFP-PfAP2-HC depletion. At 0–8 hpi in

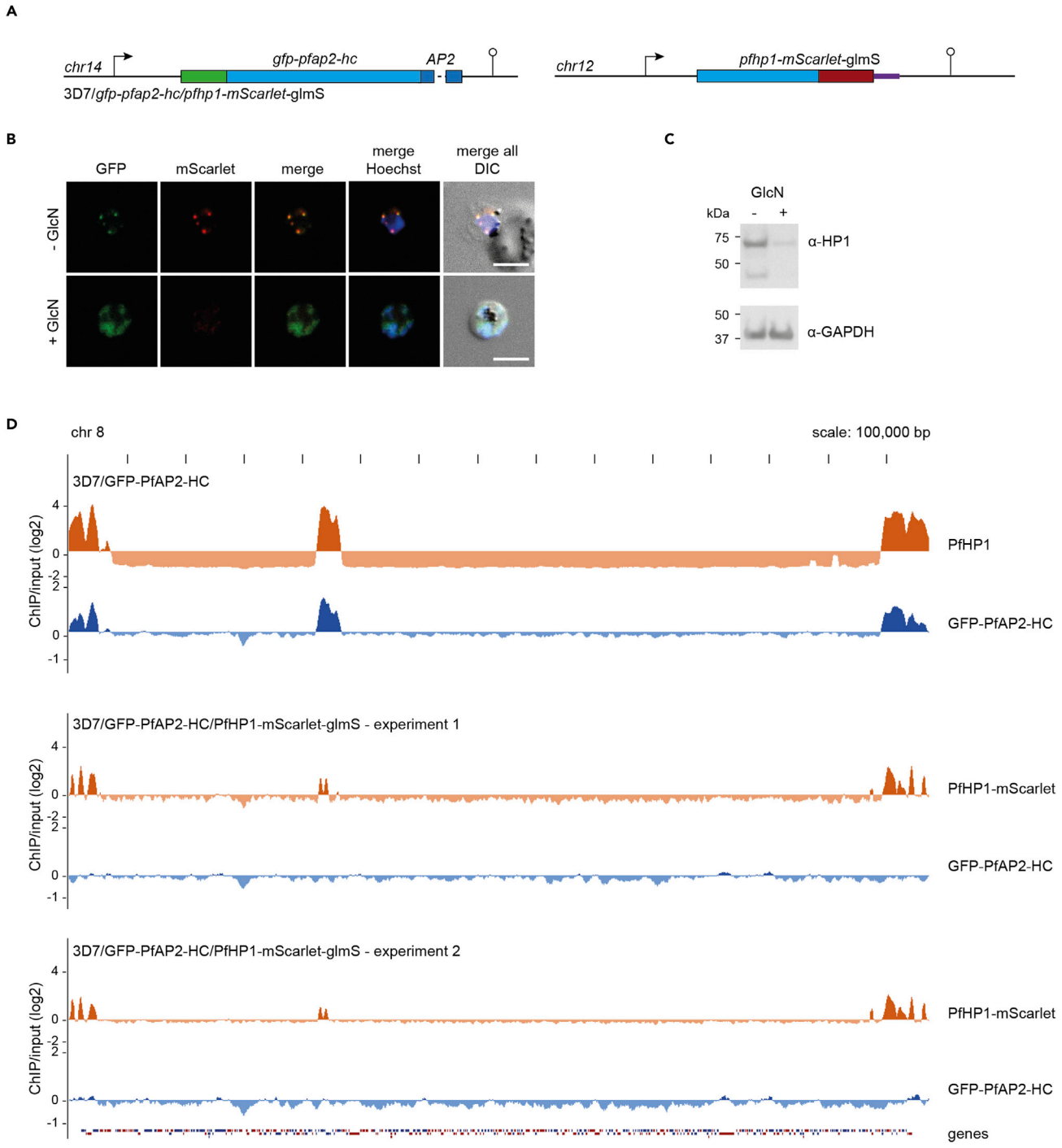

Figure 5. Binding of PfAP2-HC to heterochromatin is PfHP1 dependent

(A) Schematic maps of the endogenous *pfap2-hc* and *pfhp1* loci after CRISPR-Cas9-based editing in 3D7/GFP-PfAP2-HC/PfHP1-mScarlet-glmS parasites. The *pfap2-hc* gene was tagged with *gfp*. The *pfhp1* gene was tagged with the *mscarlet* sequence followed by a *glmS* ribozyme element to allow for detection and conditional expression of PfHP1-mScarlet, respectively. See also Figure S6.

(B) Representative live cell fluorescence images of 3D7/GFP-PfAP2-HC/PfHP1-mScarlet-glmS parasites at 32–40 hpi grown in the absence of GlcN (PfHP1 expressed) or the presence of GlcN (PfHP1 depleted). Nuclei were stained with Hoechst. DIC, differential interference contrast. Scale bar, 5 μm.

(C) Western blot showing PfHP1-mScarlet expression levels in 3D7/GFP-PfAP2-HC/PfHP1-mScarlet-glmS schizonts (36–44 hpi) grown in the absence (–) or presence (+) of GlcN. GAPDH expression levels served as a loading control. The full-sized blot is available in Figure S6.

(D) Log2-transformed α-PfHP1 (orange) and α-GFP (blue) ChIP-over-input tracks from 3D7/GFP-PfAP2-HC schizonts (top, identical to the tracks shown in Figure 1E) and from 3D7/GFP-PfAP2-HC/PfHP1-mScarlet-glmS schizonts in two independent experiments (middle and bottom).

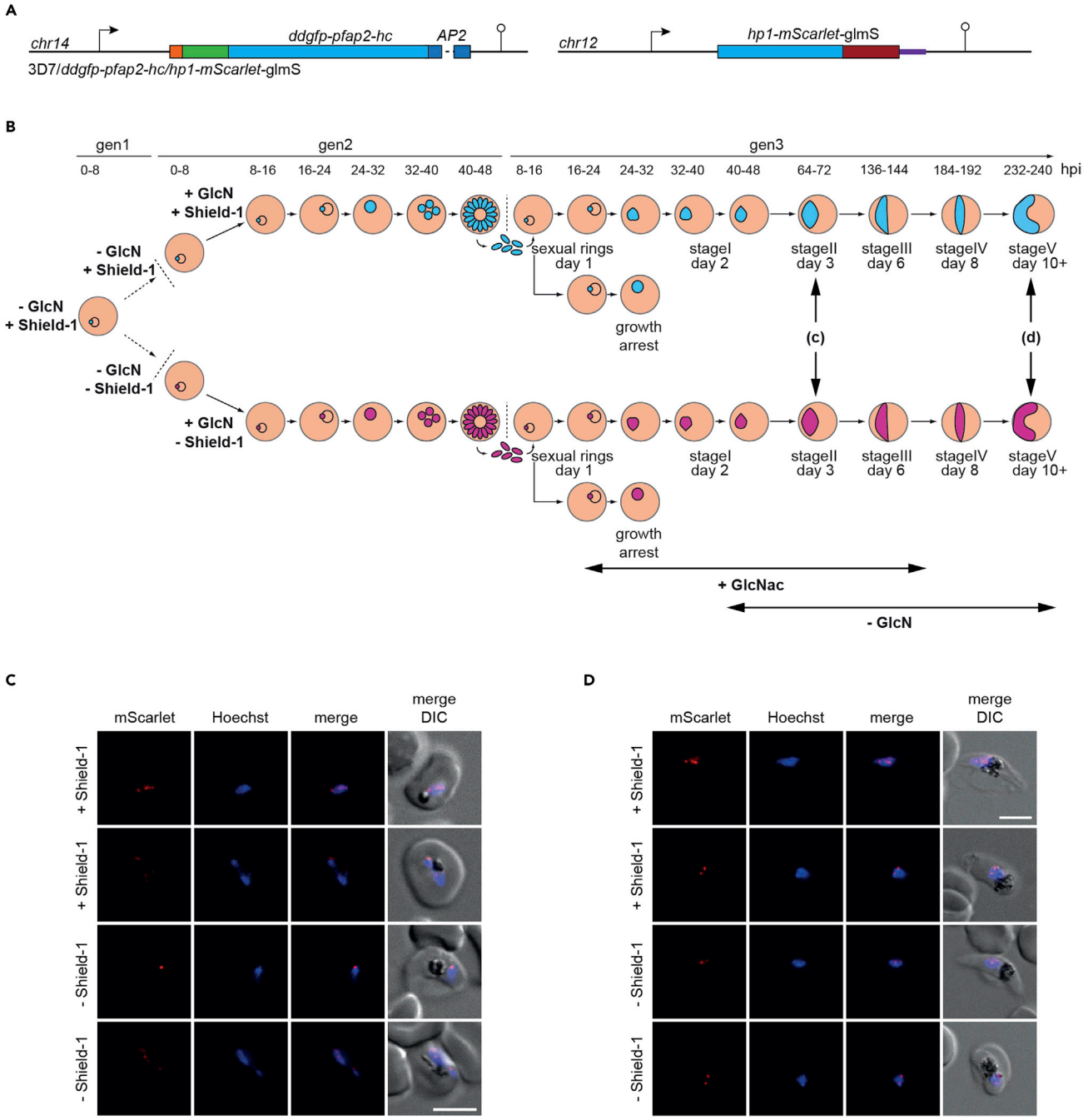

Figure 6. Depletion of PfAP2-HC has no marked effect on re-establishment of heterochromatin

(A) Schematic map of the endogenous *pfap2-hc* and *pfhp1* loci in 3D7/DDGFP-PfAP2-HC/PfHP1-mScarlet-glmS parasites after CRISPR-Cas9-mediated gene editing. The *pfap2-hc* locus was modified to introduce a *ddgfp* tag. The *pfhp1* locus was modified to contain an *mscarlet* tag followed by the *glmS* ribozyme element. See also Figure S6.

(B) Schematic detailing the design of a combined conditional DDGFP-AP2-HC depletion and PfHP1-mScarlet depletion/rescue experiment. Parasites grown in the presence of Shield-1 (+Shield-1) and the absence of glucosamine (−GlcN) exhibit stable expression of both DDGFP-PfAP2-HC and PfHP1-mScarlet. In generation 1, parasites were split into two populations at 0–8 hpi, with Shield-1 removed from one population to induce DDGFP-PfAP2-HC depletion (−Shield-1, magenta parasites) and one population maintained in the presence of Shield-1 (+Shield-1, turquoise parasites). GlcN was added to both populations at 0–8 hpi in generation 2 (+GlcN) to induce PfHP1-mScarlet depletion, which triggers sexual commitment (Brancucci et al., 2014). In generation 3, 50 mM GlcNAc was added to the ring stage cultures for 6 days to prevent growth of asexual parasites (depicted with a horizontal arrow) (Fivelman et al., 2007). Furthermore, GlcN was removed from both populations 1 day after invasion (i.e., day 2 of gametocytogenesis; stage I gametocytes) (−GlcN,

Figure 6. *Continued*
horizontal arrow) to restore PfHP1-mScarlet expression during gametocytogenesis. The double vertical arrows indicate the time points of live cell fluorescence imaging experiments to assess PfHP1-mScarlet localization in DDGFP-PfAP2-HC-expressing (+Shield-1) and -depleted (−Shield-1) parasites.
(C and D) Representative live cell fluorescence images showing PfHP1-mScarlet localization in stage II gametocytes (C) and stage V gametocytes (D) grown under DDGFP-PfAP2-HC-stabilizing (+Shield-1, upper two panels) and -depleting (−Shield-1, lower two panels) conditions. Nuclei were stained with Hoechst. DIC, differential interference contrast. Scale bar, 5 μm.

generation 2, we induced the knockdown of PfHP1-mScarlet expression in both populations through addition of GlcN (Figure 6B). Both populations (DDGFP-AP2-HC stabilized/PfHP1 depleted and DDGFP-AP2-HC depleted/PfHP1 depleted) progressed into generation 3 to produce heterochromatin-depleted sexually committed parasites and growth-arrested trophozoites. On day two of gametocytogenesis, we rescued PfHP1 expression by removal of GlcN from both parasite populations and added 50 mM N-acetyl glucosamine (GlcNac) to prevent multiplication of asexual parasites (Fivelman et al., 2007; Ponnudurai et al., 1986) that can potentially arise from arrested trophozoites resuming growth after PfHP1 rescue (Brancucci et al., 2014). We then assessed the re-establishment of perinuclear heterochromatin in the presence (+Shield-1) or absence (–Shield-1) of DDGFP-AP2-HC in stage II (64–72 hpi, day 3) (Figure 6C) and stage V (232-240 hpi, day 10) (Figure 6D) gametocytes by live cell fluorescence imaging of PfHP1-mScarlet signals. We observed no marked difference in the localization pattern of PfHP1-mScarlet between gametocytes that express or do not express DDGFP-PfAP2-HC (Figures 6C and 6D). These observations indicate that PfAP2-HC likely plays no major role in *de novo* heterochromatin formation.

DISCUSSION

Clonally variant gene expression is key to the survival of *P. falciparum* in the human host and is dependent on heterochromatin-mediated gene silencing. PfHP1, as a core component of heterochromatin, is essential for regulating processes as diverse as antigenic variation, invasion pathway switching, commitment to gametocytogenesis, and asexual proliferation (Brancucci et al., 2014; Voss et al., 2014). Our study characterizes PfAP2-HC, a member of the ApiAP2 family of putative DNA-binding proteins that specifically associates with heterochromatin throughout the genome.

Despite progress toward understanding the heterochromatic landscape of *P. falciparum*, a global view of the dynamic processes occurring to regulate and maintain heterochromatin in this parasite remains elusive. Here, we describe PfAP2-HC as an integral component of heterochromatin, only the second such factor to be characterized after gametocyte development 1 (GDV1) (Filarsky et al., 2018). GDV1 is not expressed in asexual parasites but only in parasites undergoing sexual commitment. In these cells, GDV1 binds to heterochromatin throughout the genome and destabilizes heterochromatin particularly at the *pfap2-g* locus and early gametocyte markers thus facilitating their expression (Filarsky et al., 2018). In contrast, PfAP2-HC is expressed and binds to heterochromatin in asexual parasites. Depletion of PfAP2-HC had no effect on PfHP1 localization suggesting it is not required for heterochromatin maintenance. Factors shown to date to be involved in heterochromatin maintenance in *P. falciparum* consist of histone-modifying enzymes, such as the histone deacetylase PfHda2, whose absence leads to the expression of many PfHP1-associated genes including subtelomeric multi-gene families and the internally located *pfap2-g* locus (Coleman et al., 2014). The histone deacetylases Sir2A and Sir2B are also required for maintaining *var* gene silencing but do not appear to have a role in regulating *pfap2-g* (Duraisingh et al., 2005; Tonkin et al., 2009). The incorporation of PfHP1 into heterochromatin relies on the presence of the histone post-translational modification H3K9me3 (Kwon and Workman, 2008), which is thought to be performed by the histone lysine methyltransferase (HKMT) PfSET3 in *P. falciparum* (Cui et al., 2008). PfSET3 was identified by phylogenetic analysis as a putative ortholog of the SU(VAR)3-9 HKMTs that deposit H3K9me3 marks in model eukaryotes (Cui et al., 2008). PfSET3 was indeed localized to the nuclear periphery in *P. falciparum* (Lopez-Rubio et al., 2009; Volz et al., 2010), but so far PfSET3 has not been analyzed on the functional level and methylation of H3K9 by PfSET3 could not be proven with recombinant protein assays (Cui et al., 2008). In addition to histone-modifying enzymes, other putative PfHP1-interacting factors have been identified (Filarsky et al., 2018), although their role in heterochromatin maintenance is yet to be determined. These include the chromodomain-helicase-DNA-binding protein 1 (PfCHD1), whose homologs are important in chromatin remodeling (Bugga et al., 2013; Gaspar-Maia et al., 2009); both subunits of the FACT histone chaperone, one of which was shown as vital in the production of fertile male gametes in *P. berghei* (Laurentino et al., 2011); and the Pf14-3-3I reader protein that specifically recognizes phosphorylation of serine 28 on histone 3 (Dastidar et al., 2013). The manner in which all these chromatin components interact and cooperate to mediate

reversible gene silencing in *P. falciparum* is an interesting and equally challenging question for future research.

We also tested whether the absence of PfAP2-HC may influence heterochromatin formation rather than maintenance. Because PfHP1 is essential for the proliferation of asexual parasites, we performed this experiment in gametocytes where PfHP1 is dispensable (Brancucci et al., 2014). To this end, we first depleted PfHP1 in 3D7/DDGFP-PfAP2-HC/PfHP1-mScarlet-glmS parasites through conditional knockdown of PfHP1 expression and then rescued PfHP1 expression in the sexual ring stage progeny and visualized the re-establishment of heterochromatic foci in stage II and V gametocytes by fluorescence microscopy based on PfHP1-mScarlet positivity. We did not observe any difference in the localization of PfHP1 between gametocytes expressing or not expressing PfAP2-HC. This result provides preliminary evidence suggesting that *de novo* formation of heterochromatin occurs independent of PfAP2-HC. This is in keeping with our observation that PfAP2-HC does not seem to bind chromosomal DNA *in vivo* and that the localization of PfAP2-HC is dependent on the presence of PfHP1, as discussed further below. However, we cannot exclude the possibility that a role for PfAP2-HC in nucleating heterochromatin may have been masked in this experiment by the spreading of heterochromatin from residual PfHP1 foci that remained bound to chromatin owing to incomplete PfHP1 knockdown in the asexual progenitors (Figure 5D).

We showed that the AP2 DBD of PfAP2-HC is not required for correct localization of the protein to heterochromatin. Furthermore, we could not detect direct binding of PfAP2-HC to the predicted CACACA target motifs (Campbell et al., 2010) or to other sites in chromosomal DNA *in vivo* by ChIP-seq, neither in euchromatin nor in heterochromatin, and PfAP2-HC depletion had no effect on gene transcription during the IDC. In addition, recent pull-down experiments of native nuclear proteins binding to specific DNA probes also failed to reveal an interaction of full-length PfAP2-HC with the CACACA motif (Toenhake et al., 2018). Together, these results imply that PfAP2-HC does not bind chromosomal DNA *in vivo*, suggesting functional divergence of AP2 domains within the ApiAP2 family. Although DNA-binding motifs were identified for most AP2 domains *in vitro* (Campbell et al., 2010), two of the three AP2 domains of PfAP2-I were recently shown to be dispensable in the IDC and it is unknown if they actually bind DNA *in vivo* (Santos et al., 2017). It is still possible that any direct DNA binding of PfAP2-HC was below the detection limit of our ChIP-seq experiments. However, it is perhaps more likely that PfAP2-HC indeed does not bind DNA directly *in vivo*, given its dependence on PfHP1 for correct localization. In fact, because PfAP2-HC interacts with heterochromatin independent of its AP2 domain, PfAP2-HC may actually not be meant to bind DNA directly; PfAP2-HC would likely recruit heterochromatin to any chromosomal sites it would bind to and thus potentially silence expression of genes that are important for parasite viability.

The apparent lack of DNA-binding activity displayed by the PfAP2-HC AP2 domain and the capacity of PfAP2-HC to localize to heterochromatin in absence of the AP2 domain suggest that protein-protein interactions involving the large N terminus of the protein are responsible for targeting PfAP2-HC to heterochromatin. Multiple sequence alignments of AP2-HC orthologs across all human-infecting *Plasmodium* spp. show only 30%–36% sequence identity to PfAP2-HC, and this is comparable with the AP2-HC orthologs of rodent-infecting species (31%–32%) (Figure S7). High sequence similarity is mainly confined to the AP2 domain itself, which shares $\geq$90% identical amino acids across all species (Figure S7). Of interest, there is a second semi-conserved region of 172 amino acids within PfAP2-HC with 64%–67% sequence identity to the orthologs of other human-infecting species and 53%–56% identity to those from rodent-infecting species (Figure S7), which points to an evolutionarily conserved feature. One could speculate that this region may be involved in mediating interactions with PfHP1 or other chromatin-associated factors. To date, the role of the non-AP2 region of ApiAP2 proteins has not been explicitly studied. However, given the regulatory roles PfAP2-G (Josling et al., 2020; Kafsack et al., 2014), PfAP2-I (Santos et al., 2017), and PfAP2-EXP (Martins et al., 2017) play as transcription factors, as well as the *P. berghei* ApiAP2 factors PbAP2-G (Sinha et al., 2014), PbAP2-G2 (Yuda et al., 2015), PbAP2-FG (Yuda et al., 2020), PbAP2-O (Kaneko et al., 2015; Yuda et al., 2009), PbAP2-Sp (Yuda et al., 2010), and PbAP2-L (Iwanaga et al., 2012), it can be assumed that these regions are involved in recruiting transcriptional and epigenetic machinery to the promoters in question. Indeed, coIP experiments identified the bromodomain protein PfBDP1, PfCHD1, and the FACT complex as potential interaction partners of PfAP2-I (Santos et al., 2017) and truncation of PfAP2-EXP to express only the AP2 domain led to de-regulation of its target genes (Martins et al., 2017). Functional analysis of the semi-conserved region identified in PfAP2-HC may be a promising starting point to begin understanding the role of non-AP2 domain regions in ApiAP2 factor function.

The AP2-HC factor is conserved among all *Plasmodium* spp., which clearly suggests an important role for this factor in the biology of malaria parasites, at least *in vivo*. We obtained a viable PfAP2-HC KO line that lacks any obvious phenotype in asexual blood stage parasites, but we cannot rule out functionally critical roles in other life cycle stages. Indeed, RNA-seq data show *pfap2-hc* expression in gametocyte and sporozoite stages (plasmodb.org) (Aurrecoechea et al., 2009; Gomez-Diaz et al., 2017; Lasonder et al., 2016). However, the orthologs of PfAP2-HC were successfully disrupted in the rodent malaria parasites *P. berghei* and *P. yoelii*, without discernible growth defects observed during the full life cycle in laboratory animals (Modrzynska et al., 2017; Zhang et al., 2017). These results suggest that functional redundancy or compensatory mechanisms may exist among the ApiAP2 family, as also proposed by Zhang and colleagues (Zhang et al., 2017). However, at least in asexual blood stage parasites, we believe mechanisms compensating for loss of PfAP2-HC function are highly unlikely given that the conditional knockdown of PfAP2-HC expression did not result in any transcriptional changes and caused not even a temporary defect on parasite growth or multiplication. Beyond this, it is also possible that PfAP2-HC is involved in more subtle processes not studied here, which may not present as immediate phenotypes in loss-of-function mutants but may be crucial for parasite fitness in the field. Examples of such processes are DNA repair/recombination within heterochromatic regions or epigenetic memory/switching frequencies of heterochromatic genes. The heterochromatic subtelomeric regions, which contain several hundred members of multi-copy gene families, recombine at a higher rate than the core genome in *P. falciparum*, resulting in high antigenic diversity within the parasite population (Bopp et al., 2013; Claessens et al., 2014; Frank et al., 2008). Furthermore, DNA repair mechanisms are generally less efficient in heterochromatin compared with euchromatin and thus contribute to increased mutation rates in these regions (Fortuny and Polo, 2018; Mao and Wyrick, 2019). Switches in the transcription of heterochromatic genes creates clonal variation in the expression of surface antigens, invasion factors, nutrient channels, or PfAP2-G, allowing the parasite population to adapt to and survive under adverse environmental conditions (Cortes and Deitsch, 2017; Llora-Batlle et al., 2020; Voss et al., 2014). Activation of silenced heterochromatic genes is linked to local chromatin remodeling, as demonstrated for *var* genes (Brancucci et al., 2014; Chookajorn et al., 2007; Lopez-Rubio et al., 2007), *pfap2-g* (Brancucci et al., 2014; Filarsky et al., 2018), and other clonally variant genes (Crowley et al., 2011). As an integral and specific component of heterochromatin, it is at least conceivable that PfAP2-HC may act as a positive or negative regulator of DNA repair or chromatin remodeling processes in heterochromatic regions.

In summary, our study provides a comprehensive analysis of the ApiAP2 factor PfAP2-HC, based on the analysis of six different single or double engineered transgenic parasite lines. Along with PfAP2-Tel (Sierra-Miranda et al., 2017) and PfSIP2 (Flueck et al., 2010), PfAP2-HC joins the ranks of ApiAP2 factors that do not primarily act as transcriptional regulators. We rather characterized PfAP2-HC as a PfHP1-interacting protein and core component of heterochromatin in *P. falciparum*. We found no evidence for direct binding of PfAP2-HC to chromosomal DNA *in vivo* and show that the localization of PfAP2-HC to heterochromatin is independent of the AP2 domain but strictly dependent on the presence of PfHP1. Although our efforts failed to reveal conclusive insight into PfAP2-HC function, we discovered unexpected properties of ApiAP2 factors that highlight the functional diversity among the members of this family of putative DNA-binding proteins.

Limitations of the study

As we did not observe any PfAP2-HC loss-of-function phenotypes in *P. falciparum* blood stage parasites in our study, targeted experiments in other life cycle stages will be necessary to reveal insight into the function of this ApiAP2 factor. Furthermore, although our preliminary microscopy-based data presented in Figure 6 suggest that PfAP2-HC is not involved in *de novo* heterochromatin formation, ChIP-seq and RNA-seq experiments would be required to confirm this result at higher resolution.

Resource availability

Lead contact

Further information and requests for resources and reagents should be directed to and will be fulfilled by the Lead Contact, Till Steffen Voss (till.voss@swisstph.ch).

Materials availability

Parasite lines and plasmid constructs are available from the authors upon request.

Data and code availability

The ChIP-seq and microarray data reported in this publication have been deposited in NCBI's Gene Expression Omnibus (Edgar et al., 2002) and are accessible through GEO Series accession numbers GSE154840 and GSE159061, respectively. Additional data that support the findings of this study are available in Data S1 and S2.

METHODS

All methods can be found in the accompanying Transparent methods supplemental file.

SUPPLEMENTAL INFORMATION

Supplemental information can be found online at https://doi.org/10.1016/j.isci.2021.102444.

ACKNOWLEDGMENTS

This work received funding from the Swiss National Science Foundation, Switzerland (BSCGI0_157729).

AUTHORS CONTRIBUTIONS

E.C. designed and performed experiments, analyzed and interpreted data, prepared illustrations, and wrote the manuscript. D.K. generated the 3D7/AP2-HC-KO line. R.H.M.C. and C.G.T performed high-throughput sequencing, analyzed the ChIP-seq data, and wrote the corresponding parts of the manuscript, R.B. supervised these experiments, provided resources, and wrote the corresponding parts of the manuscript. T.S.V. conceived of the study, designed and supervised experiments, provided resources, and wrote the manuscript. All authors contributed to the editing of the manuscript.

DECLARATION OF INTERESTS

The authors declare no competing interests.

Received: November 20, 2020
Revised: March 10, 2021
Accepted: April 14, 2021
Published: May 21, 2021

REFERENCES

Armstrong, C.M., and Goldberg, D.E. (2007). An FKBP destabilization domain modulates protein levels in *Plasmodium falciparum*. Nat. Methods *4*, 1007–1009.

Aurrecoechea, C., Brestelli, J., Brunk, B.P., Dommer, J., Fischer, S., Gajria, B., Gao, X., Gingle, A., Grant, G., Harb, O.S., et al. (2009). PlasmoDB: a functional genomic database for malaria parasites. Nucleic Acids Res. *37*, D539–D543.

Balaji, S., Babu, M.M., Iyer, L.M., and Aravind, L. (2005). Discovery of the principal specific transcription factors of Apicomplexa and their implication for the evolution of the AP2-integrase DNA binding domains. Nucleic Acids Res. *33*, 3994–4006.

Banaszynski, L.A., Chen, L.C., Maynard-Smith, L.A., Ooi, A.G., and Wandless, T.J. (2006). A rapid, reversible, and tunable method to regulate protein function in living cells using synthetic small molecules. Cell *126*, 995–1004.

Bartfai, R., Hoeijmakers, W.A., Salcedo-Amaya, A.M., Smits, A.H., Janssen-Megens, E., Kaan, A., Treeck, M., Gilberger, T.W., Francoijs, K.J., and Stunnenberg, H.G. (2010). H2A.Z demarcates intergenic regions of the *Plasmodium falciparum* epigenome that are dynamically marked by H3K9ac and H3K4me3. PLoS Pathog. *6*, e1001223.

Bopp, S.E., Manary, M.J., Bright, A.T., Johnston, G.L., Dharia, N.V., Luna, F.L., McCormack, S., Plouffe, D., McNamara, C.W., Walker, J.R., et al. (2013). Mitotic evolution of *Plasmodium falciparum* shows a stable core genome but recombination in antigen families. PLoS Genet. *9*, e1003293.

Brancucci, N.M.B., Bertschi, N.L., Zhu, L., Niederwieser, I., Chin, W.H., Wampfler, R., Freymond, C., Rottmann, M., Felger, I., Bozdech, Z., et al. (2014). Heterochromatin protein 1 secures survival and transmission of malaria parasites. Cell Host Microbe *16*, 165–176.

Bugga, L., McDaniel, I.E., Engie, L., and Armstrong, J.A. (2013). The *Drosophila melanogaster* CHD1 chromatin remodeling factor modulates global chromosome structure and counteracts HP1a and H3K9me2. PLoS One *8*, e59496.

Campbell, T.L., De Silva, E.K., Olszewski, K.L., Elemento, O., and Llinas, M. (2010). Identification and genome-wide prediction of DNA binding specificities for the ApiAP2 family of regulators from the malaria parasite. PLoS Pathog. *6*, e1001165.

Chookajorn, T., Dzikowski, R., Frank, M., Li, F., Jiwani, A.Z., Hartl, D.L., and Deitsch, K.W. (2007). Epigenetic memory at malaria virulence genes. Proc. Natl. Acad. Sci. U S A *104*, 899–902.

Claessens, A., Hamilton, W.L., Kekre, M., Otto, T.D., Faizullabhoy, A., Rayner, J.C., and Kwiatkowski, D. (2014). Generation of antigenic diversity in *Plasmodium falciparum* by structured rearrangement of Var genes during mitosis. PLoS Genet. *10*, e1004812.

Coleman, B.I., Skillman, K.M., Jiang, R.H., Childs, L.M., Altenhofen, L.M., Ganter, M., Leung, Y., Goldowitz, I., Kafsack, B.F., Marti, M., et al. (2014). A *Plasmodium falciparum* histone deacetylase regulates antigenic variation and gametocyte conversion. Cell Host Microbe *16*, 177–186.

Cortes, A., and Deitsch, K.W. (2017). Malaria epigenetics. Cold Spring Harb. Perspect. Med. *7*, a025528.

Crowley, V.M., Rovira-Graells, N., Ribas de, P.L., and Cortes, A. (2011). Heterochromatin formation in bistable chromatin domains controls the epigenetic repression of clonally variant *Plasmodium falciparum* genes linked to erythrocyte invasion. Mol. Microbiol. *80*, 391–406.

Cui, L., Fan, Q., and Miao, J. (2008). Histone lysine methyltransferases and demethylases in *Plasmodium falciparum*. Int. J. Parasitol. *38*, 1083–1097.

Dastidar, E.G., Dzeyk, K., Krijgsveld, J., Malmquist, N.A., Doerig, C., Scherf, A., and Lopez-Rubio, J.J. (2013). Comprehensive histone phosphorylation analysis and identification of Pf14-3-3 protein as a histone H3 phosphorylation reader in malaria parasites. PLoS One *8*, e53179.

Dietz, K.J., Vogel, M.O., and Viehhauser, A. (2010). AP2/EREBP transcription factors are part of gene regulatory networks and integrate metabolic, hormonal and environmental signals in stress acclimation and retrograde signalling. Protoplasma *245*, 3–14.

Duraisingh, M.T., and Skillman, K.M. (2018). Epigenetic variation and regulation in malaria parasites. Annu. Rev. Microbiol. *72*, 355–375.

Duraisingh, M.T., Voss, T.S., Marty, A.J., Duffy, M.F., Good, R.T., Thompson, J.K., Freitas-Junior, L.H., Scherf, A., Crabb, B.S., and Cowman, A.F. (2005). Heterochromatin silencing and locus repositioning linked to regulation of virulence genes in *Plasmodium falciparum*. Cell *121*, 13–24.

Edgar, R., Domrachev, M., and Lash, A.E. (2002). Gene Expression Omnibus: NCBI gene expression and hybridization array data repository. Nucleic. Acids Res. *30*, 207–210.

Filarsky, M., Fraschka, S.A., Niederwieser, I., Brancucci, N.M.B., Carrington, E., Carrio, E., Moes, S., Jenoe, P., Bartfai, R., and Voss, T.S. (2018). GDV1 induces sexual commitment of malaria parasites by antagonizing HP1-dependent gene silencing. Science *359*, 1259–1263.

Fivelman, Q.L., McRobert, L., Sharp, S., Taylor, C.J., Saeed, M., Swales, C.A., Sutherland, C.J., and Baker, D.A. (2007). Improved synchronous production of *Plasmodium falciparum* gametocytes in vitro. Mol. Biochem. Parasitol. *154*, 119–123.

Flueck, C., Bartfai, R., Niederwieser, I., Witmer, K., Alako, B.T., Moes, S., Bozdech, Z., Jenoe, P., Stunnenberg, H.G., and Voss, T.S. (2010). A major role for the *Plasmodium falciparum* ApiAP2 protein PfSIP2 in chromosome end biology. PLoS Pathog. *6*, e1000784.

Flueck, C., Bartfai, R., Volz, J., Niederwieser, I., Salcedo-Amaya, A.M., Alako, B.T., Ehlgen, F., Ralph, S.A., Cowman, A.F., Bozdech, Z., et al. (2009). *Plasmodium falciparum* heterochromatin protein 1 marks genomic loci linked to phenotypic variation of exported virulence factors. PLoS Pathog. *5*, e1000569.

Fortuny, A., and Polo, S.E. (2018). The response to DNA damage in heterochromatin domains. Chromosoma *127*, 291–300.

Frank, M., Kirkman, L., Costantini, D., Sanyal, S., Lavazec, C., Templeton, T.J., and Deitsch, K.W. (2008). Frequent recombination events generate diversity within the multi-copy variant antigen gene families of *Plasmodium falciparum*. Int. J. Parasitol. *38*, 1099–1109.

Fraschka, S.A., Filarsky, M., Hoo, R., Niederwieser, I., Yam, X.Y., Brancucci, N.M.B., Mohring, F., Mushunje, A.T., Huang, X., Christensen, P.R., et al. (2018). Comparative heterochromatin profiling reveals conserved and unique epigenome signatures linked to adaptation and development of malaria parasites. Cell Host Microbe *23*, 407–420.

Gaspar-Maia, A., Alajem, A., Polesso, F., Sridharan, R., Mason, M.J., Heidersbach, A., Ramalho-Santos, J., McManus, M.T., Plath, K., Meshorer, E., et al. (2009). Chd1 regulates open chromatin and pluripotency of embryonic stem cells. Nature *460*, 863–868.

Gomez-Diaz, E., Yerbanga, R.S., Lefevre, T., Cohuet, A., Rowley, M.J., Ouedraogo, J.B., and Corces, V.G. (2017). Epigenetic regulation of *Plasmodium falciparum* clonally variant gene expression during development in *Anopheles gambiae*. Sci. Rep. *7*, 40655.

Iwanaga, S., Kaneko, I., Kato, T., and Yuda, M. (2012). Identification of an AP2-family protein that is critical for malaria liver stage development. PLoS One *7*, e47557.

Jeninga, M.D., Quinn, J.E., and Petter, M. (2019). ApiAP2 transcription factors in apicomplexan parasites. Pathogens *8*, 47.

Josling, G.A., Russell, T.J., Venezia, J., Orchard, L., van Biljon, R., Painter, H.J., and Llinas, M. (2020). Dissecting the role of PfAP2-G in malaria gametocytogenesis. Nat. Commun. *11*, 1503.

Kafsack, B.F., Rovira-Graells, N., Clark, T.G., Bancells, C., Crowley, V.M., Campino, S.G., Williams, A.E., Drought, L.G., Kwiatkowski, D.P., Baker, D.A., et al. (2014). A transcriptional switch underlies commitment to sexual development in malaria parasites. Nature *507*, 248–252.

Kaneko, I., Iwanaga, S., Kato, T., Kobayashi, I., and Yuda, M. (2015). Genome-wide identification of the target genes of AP2-O, a plasmodium AP2-family transcription factor. PLoS Pathog. *11*, e1004905.

Kwon, S.H., and Workman, J.L. (2008). The heterochromatin protein 1 (HP1) family: put away a bias toward HP1. Mol. Cells *26*, 217–227.

Lasonder, E., Rijpma, S.R., van Schaijk, B.C., Hoeijmakers, W.A., Kensche, P.R., Gresnigt, M.S., Italiaander, A., Vos, M.W., Woestenenk, R., Bousema, T., et al. (2016). Integrated transcriptomic and proteomic analyses of *P. falciparum* gametocytes: molecular insight into sex-specific processes and translational repression. Nucleic Acids Res. *44*, 6087–6101.

Laurentino, E.C., Taylor, S., Mair, G.R., Lasonder, E., Bartfai, R., Stunnenberg, H.G., Kroeze, H., Ramesar, J., Franke-Fayard, B., Khan, S.M., et al. (2011). Experimentally controlled downregulation of the histone chaperone FACT in *Plasmodium berghei* reveals that it is critical to male gamete fertility. Cell. Microbiol. *13*, 1956–1974.

Llora-Batlle, O., Michel-Todo, L., Witmer, K., Toda, H., Fernandez-Becerra, C., Baum, J., and Cortes, A. (2020). Conditional expression of PfAP2-G for controlled massive sexual conversion in *Plasmodium falciparum*. Sci. Adv. *6*, eaaz5057.

Llora-Batlle, O., Tinto-Font, E., and Cortes, A. (2019). Transcriptional variation in malaria parasites: why and how. Brief Funct. Genomics *18*, 329–341.

Lopez-Rubio, J.J., Gontijo, A.M., Nunes, M.C., Issar, N., Hernandez, R.R., and Scherf, A. (2007). 5′ flanking region of var genes nucleate histone modification patterns linked to phenotypic inheritance of virulence traits in malaria parasites. Mol. Microbiol. *66*, 1296–1305.

Lopez-Rubio, J.J., Mancio-Silva, L., and Scherf, A. (2009). Genome-wide analysis of heterochromatin associates clonally variant gene regulation with perinuclear repressive centers in malaria parasites. Cell Host Microbe *5*, 179–190.

Mao, P., and Wyrick, J.J. (2019). Organization of DNA damage, excision repair, and mutagenesis in chromatin: a genomic perspective. DNA Repair (Amst). *81*, 102645.

Martins, R.M., Macpherson, C.R., Claes, A., Scheidig-Benatar, C., Sakamoto, H., Yam, X.Y., Preiser, P., Goel, S., Wahlgren, M., Sismeiro, O., et al. (2017). An ApiAP2 member regulates expression of clonally variant genes of the human malaria parasite *Plasmodium falciparum*. Sci. Rep. *7*, 14042.

Modrzynska, K., Pfander, C., Chappell, L., Yu, L., Suarez, C., Dundas, K., Gomes, A.R., Goulding, D., Rayner, J.C., Choudhary, J., et al. (2017). A knockout screen of ApiAP2 genes reveals networks of interacting transcriptional regulators controlling the plasmodium life cycle. Cell Host Microbe *21*, 11–22.

Painter, H.J., Campbell, T.L., and Llinas, M. (2011). The Apicomplexan AP2 family: integral factors regulating Plasmodium development. Mol. Biochem. Parasitol. *176*, 1–7.

Perez-Toledo, K., Rojas-Meza, A.P., Mancio-Silva, L., Hernandez-Cuevas, N.A., Delgadillo, D.M., Vargas, M., Martinez-Calvillo, S., Scherf, A., and Hernandez-Rivas, R. (2009). *Plasmodium falciparum* heterochromatin protein 1 binds to tri-methylated histone 3 lysine 9 and is linked to mutually exclusive expression of var genes. Nucleic Acids Res. *37*, 2596–2606.

Ponnudurai, T., Lensen, A.H., Meis, J.F., and Meuwissen, J.H. (1986). Synchronization of *Plasmodium falciparum* gametocytes using an automated suspension culture system. Parasitology *93*, 263–274.

Prommana, P., Uthaipibull, C., Wongsombat, C., Kamchonwongpaisan, S., Yuthavong, Y., Knuepfer, E., Holder, A.A., and Shaw, P.J. (2013). Inducible knockdown of Plasmodium gene expression using the glmS ribozyme. PLoS One *8*, e73783.

Rovira-Graells, N., Gupta, A.P., Planet, E., Crowley, V.M., Mok, S., Ribas de Pouplana, L., Preiser, P.R., Bozdech, Z., and Cortes, A. (2012). Transcriptional variation in the malaria parasite *Plasmodium falciparum*. Genome Res. *22*, 925–938.

Sadaie, M., Iida, T., Urano, T., and Nakayama, J. (2004). A chromodomain protein, Chp1, is required for the establishment of heterochromatin in fission yeast. EMBO J. *23*, 3825–3835.

Salcedo-Amaya, A.M., van Driel, M.A., Alako, B.T., Trelle, M.B., van den Elzen, A.M., Cohen, A.M., Janssen-Megens, E.M., van de Vegte-Bolmer, M., Selzer, R.R., Iniguez, A.L., et al. (2009). Dynamic histone H3 epigenome marking during

the intraerythrocytic cycle of *Plasmodium falciparum*. Proc. Natl. Acad. Sci. U S A *106*, 9655–9660.

Santos, J.M., Josling, G., Ross, P., Joshi, P., Orchard, L., Campbell, T., Schieler, A., Cristea, I.M., and Llinas, M. (2017). Red blood cell invasion by the malaria parasite is coordinated by the PfAP2-I transcription factor. Cell Host Microbe *21*, 731–741.

Scherf, A., Lopez-Rubio, J.J., and Riviere, L. (2008). Antigenic variation in *Plasmodium falciparum*. Annu. Rev. Microbiol. *62*, 445–470.

Sierra-Miranda, M., Vembar, S.S., Delgadillo, D.M., Avila-Lopez, P.A., Herrera-Solorio, A.M., Lozano, A.D., Vargas, M., and Hernandez-Rivas, R. (2017). PfAP2Tel, harbouring a non-canonical DNA-binding AP2 domain, binds to *Plasmodium falciparum* telomeres. Cell. Microbiol. *19*. https://doi.org/10.1111/cmi.12742.

Sinha, A., Hughes, K.R., Modrzynska, K.K., Otto, T.D., Pfander, C., Dickens, N.J., Religa, A.A., Bushell, E., Graham, A.L., Cameron, R., et al. (2014). A cascade of DNA-binding proteins for sexual commitment and development in Plasmodium. Nature *507*, 253–257.

Toenhake, C.G., Fraschka, S.A., Vijayabaskar, M.S., Westhead, D.R., van Heeringen, S.J., and Bartfai, R. (2018). Chromatin accessibility-based characterization of the gene regulatory network underlying *Plasmodium falciparum* blood-stage development. Cell Host Microbe *23*, 557–569 e559.

Tonkin, C.J., Carret, C.K., Duraisingh, M.T., Voss, T.S., Ralph, S.A., Hommel, M., Duffy, M.F., Silva, L.M., Scherf, A., Ivens, A., et al. (2009). Sir2 paralogues cooperate to regulate virulence genes and antigenic variation in *Plasmodium falciparum*. PLoS Biol. *7*, e84.

Venugopal, K., Hentzschel, F., Valkiunas, G., and Marti, M. (2020). Plasmodium asexual growth and sexual development in the haematopoietic niche of the host. Nat. Rev. Microbiol. *18*, 177–189.

Volz, J., Carvalho, T.G., Ralph, S.A., Gilson, P., Thompson, J., Tonkin, C.J., Langer, C., Crabb, B.S., and Cowman, A.F. (2010). Potential epigenetic regulatory proteins localise to distinct nuclear sub-compartments in *Plasmodium falciparum*. Int. J. Parasitol. *40*, 109–121.

Voss, T.S., Bozdech, Z., and Bartfai, R. (2014). Epigenetic memory takes center stage in the survival strategy of malaria parasites. Curr. Opin. Microbiol. *20*, 88–95.

Watson, P.Y., and Fedor, M.J. (2011). The glmS riboswitch integrates signals from activating and inhibitory metabolites in vivo. Nat. Struct. Mol. Biol. *18*, 359–363.

WHO (2019). World Malaria Report 2019 (World Health Organisation).

Yuda, M., Iwanaga, S., Kaneko, I., and Kato, T. (2015). Global transcriptional repression: an initial and essential step for Plasmodium sexual development. Proc. Natl. Acad. Sci. U S A *112*, 12824–12829.

Yuda, M., Iwanaga, S., Shigenobu, S., Kato, T., and Kaneko, I. (2010). Transcription factor AP2-Sp and its target genes in malarial sporozoites. Mol. Microbiol. *75*, 854–863.

Yuda, M., Iwanaga, S., Shigenobu, S., Mair, G.R., Janse, C.J., Waters, A.P., Kato, T., and Kaneko, I. (2009). Identification of a transcription factor in the mosquito-invasive stage of malaria parasites. Mol. Microbiol. *71*, 1402–1414.

Yuda, M., Kaneko, I., Iwanaga, S., Murata, Y., and Kato, T. (2020). Female-specific gene regulation in malaria parasites by an AP2-family transcription factor. Mol. Microbiol. *113*, 40–51.

Zhang, C., Li, Z., Cui, H., Jiang, Y., Yang, Z., Wang, X., Gao, H., Liu, C., Zhang, S., Su, X.Z., et al. (2017). Systematic CRISPR-cas9-mediated modifications of *Plasmodium yoelii* ApiAP2 genes reveal functional insights into parasite development. mBio *8*, e01986–17.

iScience, Volume *24*

Supplemental information

The ApiAP2 factor PfAP2-HC is an integral component of heterochromatin in the malaria parasite *Plasmodium falciparum*

Eilidh Carrington, Roel Henrikus Martinus Cooijmans, Dominique Keller, Christa Geeke Toenhake, Richárd Bártfai, and Till Steffen Voss

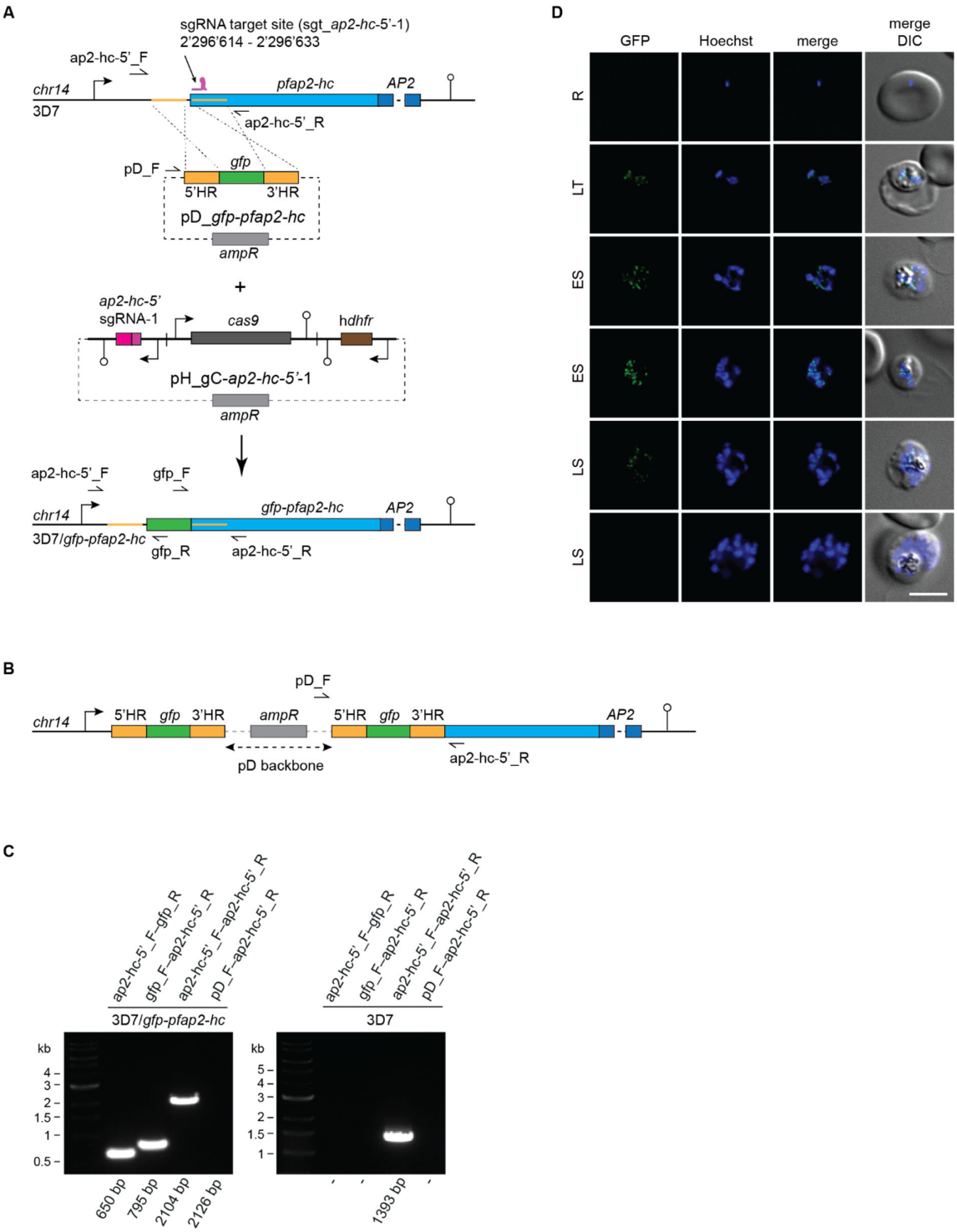

Figure S1. Generation of the 3D7/GFP-PfAP2-HC parasite line and live cell fluorescence imaging, Related to Figure 1

(A) Schematic maps of the *pfap2-hc* locus (PF3D7_1456000) in 3D7 parasites (top), the CRISPR/Cas9 transfection vectors pD_*gfp-pfap2-hc* and pH_gC-*ap2-hc-5'*-1 (centre), and the modified *pfap2-hc* locus after CRISPR/Cas9-based genome editing in 3D7/GFP-PfAP2-HC parasites (bottom). The AP2 DBD-encoding sequence, which is interrupted by an intron, is indicated (AP2, dark blue). The position of the sgt_*ap2-hc-5'*-1 sgRNA target sequence is indicated (chromosome 14 coordinates). The pD_*gfp-pfap2-hc* donor plasmid contains a *gfp* sequence (green) flanked by homology regions (HR, yellow) for homology-directed repair. The pH_gC-*ap2-hc-5'*-1 plasmid contains expression cassettes for SpCas9 (dark grey), the sgRNA (pink) and the h*dhfr* resistance marker

(brown). Successful gene editing results in the expression of an N-terminally tagged GFP-PfAP2-HC protein. PCR primer binding sites are indicated by arrows and were used to confirm successful gene editing.
(B) Schematic map of the modified *pfap2-hc* locus after CRISPR/Cas9-based genome editing in the event of donor plasmid concatemer integration into the genome. PCR primer binding sites are indicated by arrows and were used to check for donor plasmid concatemer integration.
(C) PCR on gDNA from a 3D7/GFP-PfAP2-HC clone and 3D7 wild-type parasites. Primers ap2-hc-5'_F and ap2-hc-5'_R bind to chromosomal sequences outside the HRs and amplify a 2104 bp or 1393 bp fragment from the edited or wild-type *pfap2-hc* locus, respectively. The ap2-hc-5'_F-gfp_R and gfp_F-ap2-hc-5'_R primer combinations are specific for the edited locus and amplify 650 bp and 795 bp fragments, respectively. Primer pD_F binds to the donor plasmid backbone and, when used in combination with primer ap2-hc-5'_R, will amplify a fragment of 2126 bp if a donor plasmid concatemer was integrated into the genome.
(D) Live cell fluorescence imaging of 3D7/GFP-PfAP2-HC parasites throughout the IDC. R, ring stage. LT, late trophozoite with two parasites infecting one RBC. ES, early schizont. LS, late schizont. Nuclei were stained with Hoechst. DIC, differential interference contrast. Scale bar, 5 µm.

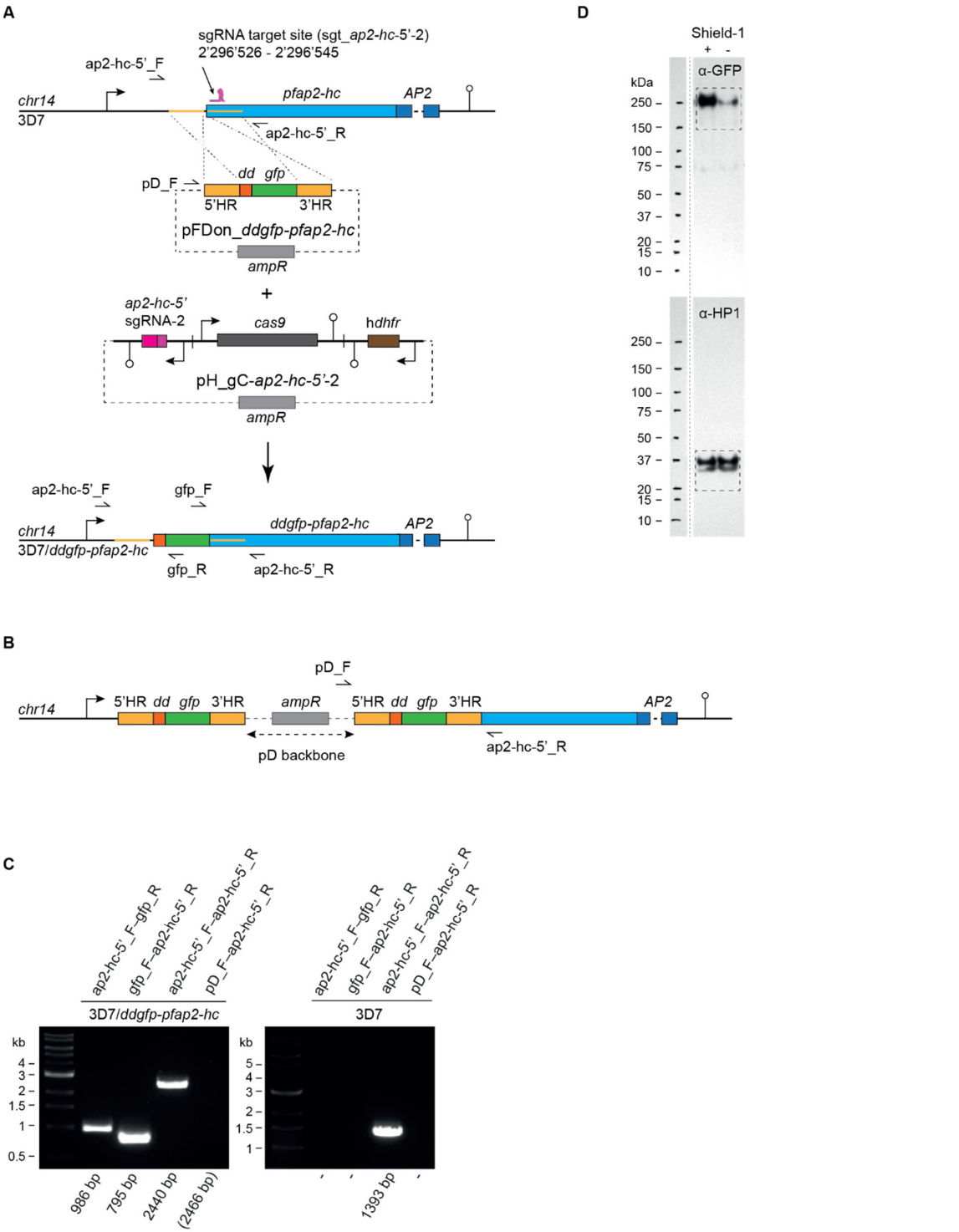

Figure S2. Generation of the 3D7/DDGFP-PfAP2-HC parasite line, Related to Figure 2
(A) Schematic maps of the *pfap2-hc* locus (PF3D7_1456000) in 3D7 parasites (top), the CRISPR/Cas9 transfection vectors pFDon_*ddgfp-pfap2-hc* and pH_gC-*ap2-hc-5'*-2 (centre), and the modified *pfap2-hc* locus after CRISPR/Cas9-based genome editing in 3D7/DDGFP-PfAP2-HC parasites (bottom). The AP2 DBD-encoding sequence, which is interrupted by an intron, is indicated (AP2, dark blue). The position of the sgt_*ap2-hc-5'*-1 sgRNA target sequence is indicated (chromosome 14 coordinates). The pFDon_*ddgfp-pfap2-hc* donor plasmid contains an FKBP destabilisation domain (*dd*, orange) and *gfp* sequence (green) flanked by homology regions (HR, yellow) for homology-directed repair. The pH_gC-*ap2-hc-5'*-2 plasmid contains expression cassettes for SpCas9 (dark grey), the sgRNA (pink) and the h*dhfr* resistance marker (brown). Successful gene

editing results in the expression of an N-terminally tagged DDGFP-PfAP2-HC protein. PCR primer binding sites are indicated by half arrows and were used to confirm successful gene editing.
(B) Schematic map of the modified *pfap2-hc* locus after CRISPR/Cas9-based genome editing in the event of donor plasmid concatemer integration into the genome. PCR primer binding sites are indicated by arrows and were used to check for donor plasmid concatemer integration.
(C) PCR on gDNA from a 3D7/DDGFP-PfAP2-HC clone and 3D7 wild-type parasites. Primers ap2-hc-5'_F and ap2-hc-5'_R bind to chromosomal sequences outside the HRs and amplify a 2440 bp or 1393 bp fragment from the edited or wild-type *pfap2-hc* locus, respectively. The ap2-hc-5'_F-gfp_R and gfp_F-ap2-hc-5'_R primer combinations are specific for the edited locus and amplify 986 bp and 795 bp fragments, respectively. Primer pD_F binds to the donor plasmid backbone and, when used in combination with primer ap2-hc-5'_R, will amplify a fragment of 2466 bp if a donor plasmid concatemer was integrated into the genome.
(D) Full sized Western blot of the sections shown in Figure 2C showing DDGFP-PfAP2-HC expression levels in 3D7/DDGFP-PfAP2-HC parasites grown in the presence (+) or absence (-) of Shield-1. The membrane was first probed with α-GFP antibodies (top) before inactivation of horseradish peroxidase with 2 mM NaN_3, followed by re-probing with the α-PfHP1 antibodies (bottom) used as a loading control. Dashed boxes show the sections presented in Figure 2C.

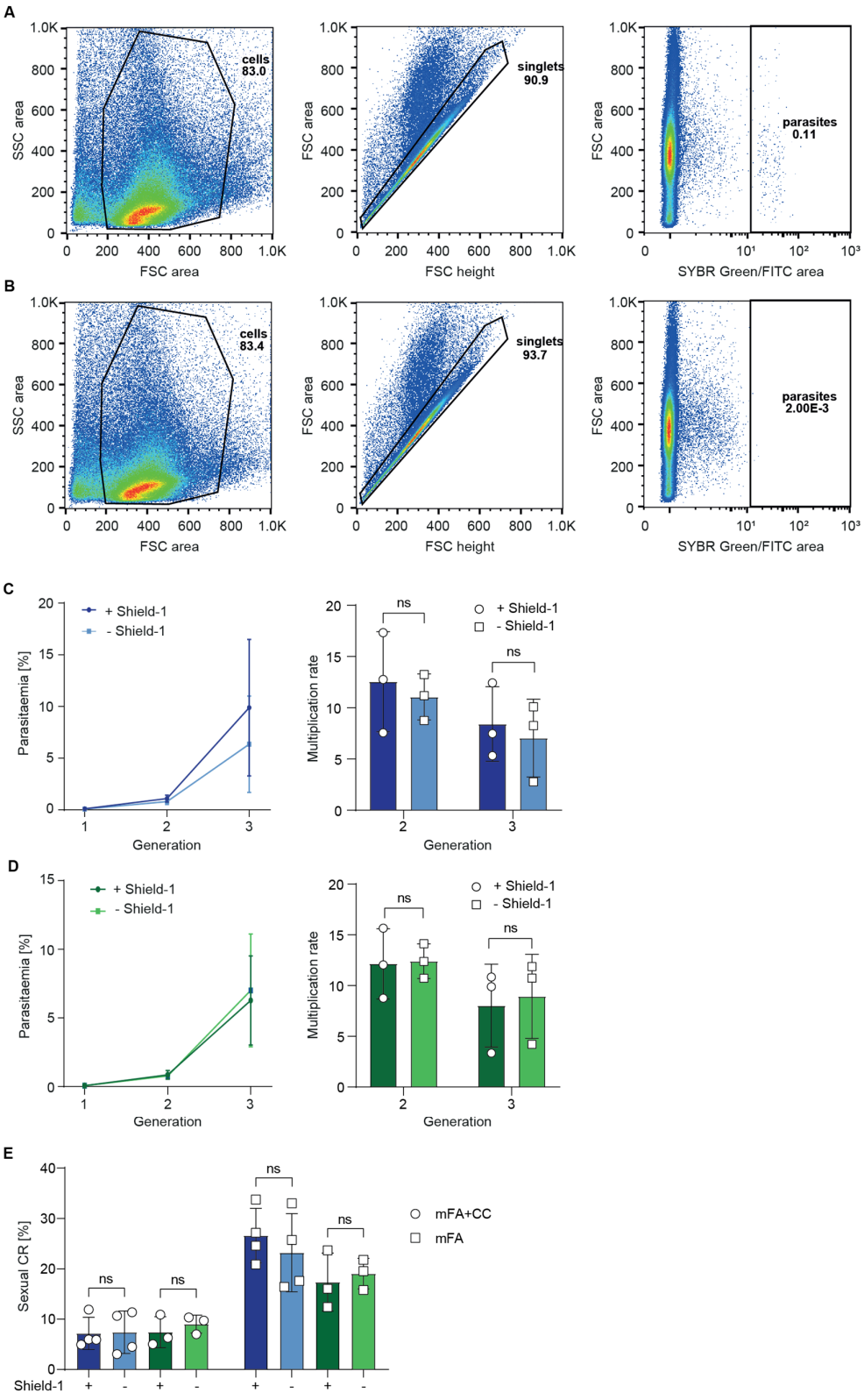

Figure S3. Multiplication rates and gametocyte conversion rates of 3D7/DDGFP-PfAP2-HC parasites, Related to Figure 2

(A, B) Gating strategy applied to flow cytometry data obtained from multiplication assays. Representative flow cytometry plots of an infected (3D7/WT, – Shield-1, panel A) and uninfected RBC control sample (panel B) measured on day 1 of the multiplication assay. The first plot shows the gate

to remove debris smaller than cell size to include only the ‘cells’ population. The second plot shows the gate to include only single measurement events, termed ‘singlets’, and the third gate separates uninfected from infected RBCs based on the SYBR Green intensity of the uninfected RBC control, termed ‘parasites’. The numbers are the percentage of events included within the gate, with the final gate ‘parasites’ reflecting the parasitaemia of the sample. This gating strategy was applied to all flow cytometry data shown in panels C and D, and in Figure S4.
(C, D) Flow cytometry data showing the increase in parasitaemia (left) and parasite multiplication rates (right) in two subsequent generations of 3D7/DDGFP-PfAP2-HC (panel C) parasites grown in the presence (+, dark blue) or absence (–, light blue) of Shield-1 and 3D7/WT (panel D) parasites grown in the presence (+, dark green) or absence (–, light green) of Shield-1. The mean ±SD of three biological replicates are shown. Data points of individual replicates are shown for parasite multiplication rates and represented by open circles (+ Shield-1) or open squares (– Shield-1). ns, not significant (paired two-tailed Student’s t test).
(E) Sexual conversion rates of 3D7/DDGFP-PfAP2-HC (dark/light blue) and 3D7/WT (dark/light green) parasites exposed to mFA+CC medium (conditions inhibiting sexual commitment, open circles) or mFA medium (conditions inducing sexual commitment, open squares) (Brancucci et al., 2017). Parasites grown in the presence (+) or absence (–) of Shield-1 are compared. The mean ±SD of four biological replicates of 3D7/DDGFP-PfAP2-HC and three biological replicates of 3D7/WT are shown. Data points of individual replicates are shown. ns, not significant (paired two-tailed Student’s t test). CR, conversion rate.

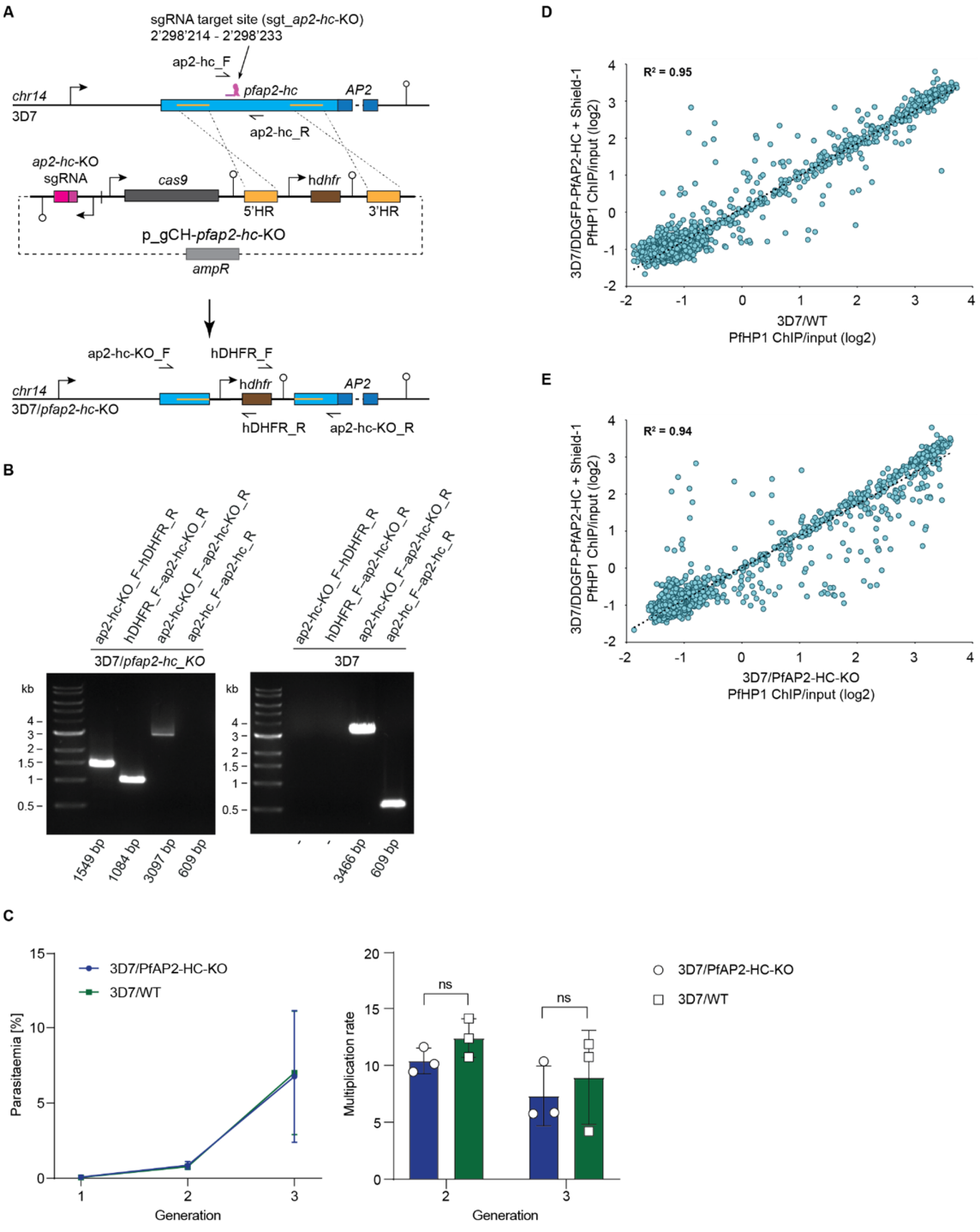

Figure S4. Generation of the 3D7/PfAP2-HC-KO parasite line, Related to Figure 2
(A) Schematic maps of the *pfap2-hc* locus (PF3D7_1456000) in 3D7 parasites (top), the p_gCH-*pfap2-hc*-KO transfection vector (centre), and the modified *pfap2-hc* locus after CRISPR/Cas9-based genome editing in 3D7/PfAP2-HC-KO parasites (bottom). The AP2 DBD-encoding sequence, which is interrupted by an intron, is indicated (AP2, dark blue). The position of the sgt_*ap2-hc*-KO sgRNA target sequence is indicated (chromosome 14 coordinates). The p_gCH-*pfap2-hc*-KO plasmid contains expression cassettes for SpCas9 (dark grey), the sgRNA (pink) and the h*dhfr* resistance marker (brown) flanked by two homology regions (HR, yellow) for homology-directed repair. Successful gene editing results in the h*dhfr* expression cassette replacing a section of the *pfap2-hc* gene, disrupting its expression. PCR primer binding sites are indicated by arrows and were used to confirm successful gene editing.

(B) PCR on gDNA from 3D7/PfAP2-HC-KO and 3D7 wild-type parasites. Primers ap2-hc-KO_F and ap2-hc-KO_R bind to chromosomal sequences outside the HRs and amplify a 3097 bp or 3466 bp fragment from the edited or wild-type *pfap2-hc* locus, respectively. The ap2-hc-KO_F-hDHFR_R and hDHFR_F-ap2-hc-KO_R primer combinations are specific for the edited locus and amplify 1549 bp and 1084 bp fragments, respectively. Primer combination ap2-hc_F-ap2-hc_R is specific for the wild-type locus and amplifies a 609 bp fragment.
(C) Flow cytometry data showing the increase in parasitaemia (left) and parasite multiplication rates (right) in two subsequent generations of 3D7/PfAP2-HC-KO (dark blue) and 3D7/WT (dark green) parasites. The 3D7/WT data is identical to those shown in Figure S2D (3D7/WT grown in the absence of Shield-1). The mean ±SD of three biological replicates are shown. Data points of individual replicates are shown for parasite multiplication rates and represented by open circles (3D7/PfAP2-HC-KO) or open squares (3D7/WT). ns, not significant (paired two-tailed Student's t test).
(D, E) Scatterplots of average log2-transformed α-PfHP1 ChIP/input values for all parasite genes in 3D7/WT and 3D7/DDGFP-PfAP2-HC schizonts grown in the presence (+) of Shield-1 (panel C) and in 3D7/PfAP2-HC-KO and 3D7/DDGFP-PfAP2-HC schizonts grown in the presence (+) of Shield-1 (panel D). Depicted regression lines are based on heterochromatic genes only (log2 ratio α-PfHP1/input ≥ 0). The coefficients of determination (R^2) are shown on the top left.

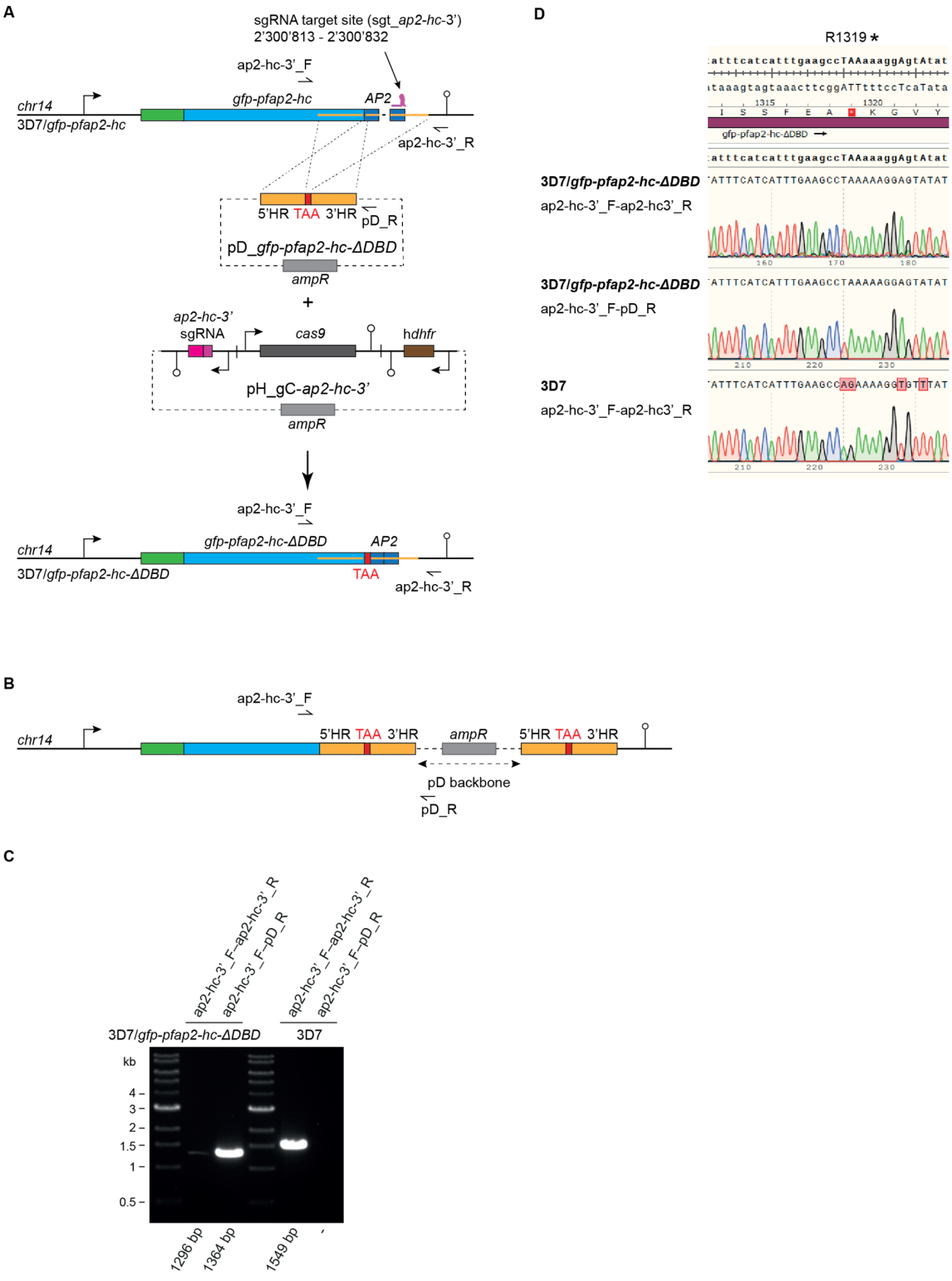

Figure S5. Generation of the 3D7/GFP-PfAP2-HC-ΔDBD parasite line, Related to Figure 4
(A) Schematic maps of the *gfp-pfap2-hc* locus in 3D7/GFP-PfAP2-HC parasites (top, see Figure S1), the CRISPR/Cas9 transfection vectors pD_*gfp-pfap2-hc-ΔDBD* and pH_gC-*ap2-hc-3'* (centre), and the modified *gfp-pfap2-hc* locus after CRISPR/Cas9-based genome editing in 3D7/GFP-PfAP2-HC-ΔDBD parasites (bottom). The AP2 DBD-encoding sequence, which is interrupted by an intron, is indicated (AP2, dark blue). The position of the sgt_*ap2-hc-3'* sgRNA target sequence is indicated (chromosome 14 coordinates). The pD_*gfp-pfap2-hc-ΔDBD* donor plasmid contains a premature TAA stop codon

(red) flanked by homology regions (HR, yellow) for homology-directed repair. The pH_gC-*ap2-hc-3'* plasmid contains expression cassettes for SpCas9 (dark grey), the sgRNA (pink) and the h*dhfr* resistance marker (brown). Successful gene editing results in the expression of a truncated GFP-PfAP2-HC protein lacking the AP2 DNA-binding domain (GFP-PfAP2-HC-ΔDBD). PCR primer binding sites are indicated by arrows and were used to confirm successful gene editing.
(B) Schematic map of the modified *gfp-pfap2-hc* locus after CRISPR/Cas9-based genome editing in the event of donor plasmid concatemer integration into the genome. PCR primer binding sites are indicated by arrows and were used to check for donor plasmid concatemer integration.
(C) PCR on gDNA from 3D7/GFP-PfAP2-HC-ΔDBD and 3D7 wild-type parasites. Primers ap2-hc-3'_F and ap2-hc-3'_R bind to chromosomal sequences outside the HRs and amplify a 1296 bp or 1549 bp fragment from the edited or wild-type *pfap2-hc* locus, respectively. Primer pD_R binds to the donor plasmid backbone and, when used in combination with primer ap2-hc-3'_F, amplifies a fragment of 1364 bp if a donor plasmid concatemer was integrated into the genome.
(D) Sanger sequencing of the two PCR products ap2-hc-3'_F-ap2-hc-3'_R (top) and ap2-hc-3'_F-pD_R (middle) amplified from 3D7/GFP-PfAP2-HC-ΔDBD parasites (see panel B, lanes 2 and 3) confirms the successful introduction of the AG→TA double mutation creating a premature STOP codon (R1319*). The PCR product ap2-hc-3'_F-ap2-hc-3'_R (bottom) amplified from 3D7 wild-type parasites (see panel B, lane 5) shows the wild-type sequence. Additional mutations downstream of the AG→TA double mutation are part of the re-codonised sequence introduced to avoid homologues recombination at an undesired location to ensure correct CRISPR/Cas9 genome editing.

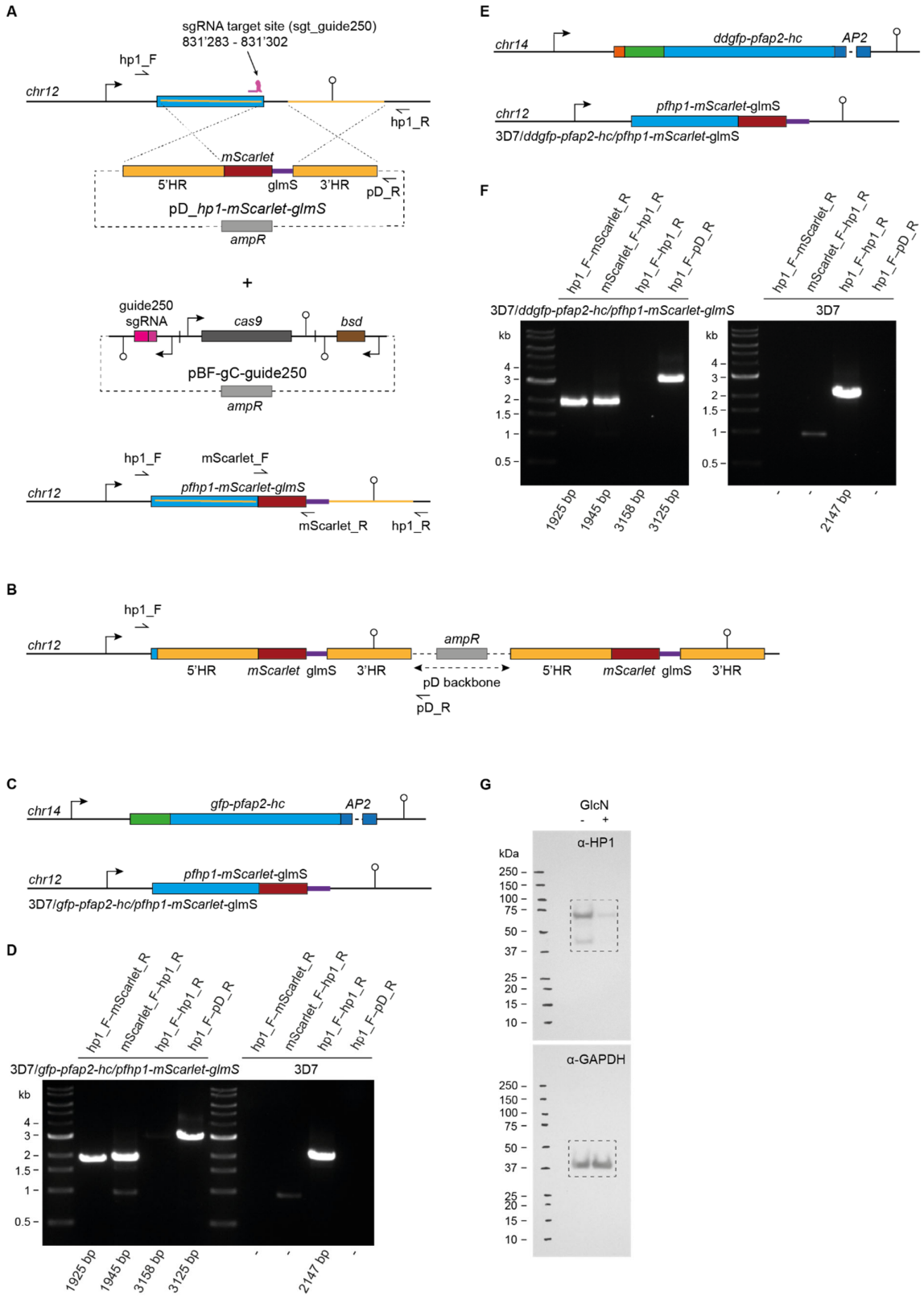

Figure S6. Generation of the 3D7/GFP-PfAP2-HC/PfHP1-mScarlet-glmS and 3D7/DDGFP-PfAP2-HC/PfHP1-mScarlet-glmS parasite lines, Related to Figures 5 and 6

(A) Schematic maps of the wild-type *pfhp1* locus (PF3D7_1220900) in 3D7/GFP-PfAP2-HC and 3D7/DDGFP-PfAP2-HC parasites (top), the CRISPR/Cas9 transfection vectors pD_*hp1-mScarlet-glmS* and pBF-gC-guide250 (Bui et al., 2019) (centre), and the modified *pfhp1* locus after

CRISPR/Cas9-based genome editing (bottom). The position of the sgt_guide250 sgRNA target sequence is indicated (chromosome 12 coordinates). The pD_*hp1-mScarlet-glmS* donor plasmid contains the *mScarlet* sequence (*red*) followed by the *glmS* ribozyme sequence (purple) flanked by homology regions (HR, yellow) for homology-directed repair. The pBF-gC-guide250 plasmid (Bui et al., 2019) contains expression cassettes for SpCas9 (dark grey), the sgRNA (pink) and the blasticidin deaminase (*bsd*) resistance marker (brown). Successful gene editing results in the expression of a C-terminally tagged PfHP1-mScarlet protein controlled by the *glmS* ribozyme element. PCR primer binding sites are indicated by half arrows and were used to confirm successful gene editing.
(B) Schematic map of the modified *pfhp1* locus after CRISPR/Cas9-based genome editing in the event of donor plasmid concatemer integration into the genome. PCR primer binding sites are indicated by arrows and were used to check for donor plasmid concatemer integration.
(C) Schematic maps of the *gfp-pfap2-hc* locus (top, see Figure S1) and the *pfhp1-mScarlet-glmS* locus (bottom) in successfully edited 3D7/GFP-PfAP2-HC/PfHP1-mScarlet-glmS parasites.
(D) PCR on gDNA from 3D7/GFP-PfAP2-HC/PfHP1-mScarlet-glmS and 3D7 wild-type parasites. Primers hp1_F and hp1_R bind to chromosomal sequences outside the HRs and amplify a 3158 bp or 2147 bp fragment from the edited or wild-type *pfhp1* locus, respectively. The hp1_F-mScarlet_R and mScarlet_F-hp1_R primer combinations are specific for the edited locus and amplify 1925 bp and 1945 bp fragments, respectively. Primer pD_R binds to the donor plasmid backbone and, when used in combination with primer hp1_F, will amplify a fragment of 3125 bp if a donor plasmid concatemer was integrated into the genome.
(E) Schematic maps of the *ddgfp-pfap2-hc* locus (top, see Figure S2) and the *pfhp1-mScarlet-glmS* locus (bottom) in successfully edited 3D7/DDGFP-PfAP2-HC/PfHP1-mScarlet-glmS parasites.
(F) PCR on gDNA from 3D7/DDGFP-PfAP2-HC/PfHP1-mScarlet-glmS and 3D7 wild-type parasites. Primer explanations are as in panel D. Primer combination mScarlet_F-hp1_R results in a faint non-specific product at ~1000 bp in all reactions (panels D and F).
(G) Full sized Western blot of the sections shown in Figure 5C showing PfHP1-mScarlet expression levels in 3D7/GFP-PfAP2-HC/PfHP1-mScarlet-glmS parasites grown in the absence (–) or presence (+) of GlcN. The membrane was first probed with α-PfHP1 antibodies (top) before inactivation of horseradish peroxidase with 2 mM NaN_3, followed by re-probing with the α-GAPDH antibodies (bottom) used as a loading control. Dashed boxes show the sections presented in Figure 5C.

A

B

1 – 1374: Full length, % sequence identity								
	Pv	**Pk**	**Poc**	**Pm**	**Pb**	**Py**	**Pc**	**Pf**
Pv	100	81	46	46	37	38	37	35
Pk	81	100	47	46	37	37	36	35
Poc	46	47	100	46	37	38	38	31
Pm	46	46	46	100	40	41	40	34
Pb	37	37	37	40	100	91	83	32
Py	38	37	38	41	91	100	85	33
Pc	37	36	38	40	83	85	100	31
Pf	35	35	31	34	32	33	31	100

C

955 – 1126: Semi-conserved domain, % sequence identity								
	Pm	**Poc**	**Pv**	**Pk**	**Pf**	**Pb**	**Py**	**Pc**
Pm	100	78	77	76	64	62	64	62
Poc	78	100	76	75	67	59	60	60
Pv	77	76	100	95	66	58	60	59
Pk	76	75	95	100	66	59	60	59
Pf	64	67	66	66	100	53	56	55
Pb	62	59	58	59	53	100	95	92
Py	64	60	60	60	56	95	100	95
Pc	62	60	59	59	55	92	95	100

D

1297 – 1374: AP2 domain, % sequence identity								
	Pb	**Pc**	**Py**	**Pm**	**Poc**	**Pv**	**Pk**	**Pf**
Pb	100	99	99	94	94	95	95	90
Pc	99	100	100	95	95	96	96	91
Py	99	100	100	95	95	96	96	91
Pm	94	95	95	100	97	99	99	94
Poc	94	95	95	97	100	96	96	94
Pv	95	96	96	99	96	100	100	95
Pk	95	96	96	99	96	100	100	95
Pf	90	91	91	94	94	95	95	100

Figure S7. AP2-HC amino acid sequence comparison between orthologs of different *Plasmodium* species, Related to Figures 4 and 5

(A) Schematic map of the PfAP2-HC protein showing the location of the AP2 domain (blue) and a semi-conserved domain (green) identified via a multiple sequence alignment of AP2-HC orthologues from *P. vivax* (PVX_117665), *P. knowlesi* (PKNH_1225800), *P. malariae* (PmUG01_12060900), *P. ovale curtisi* (PocGH01_12058800), *P. berghei* (PBANKA_1319700), *P. yoelii* (PY17X_1323500) and *P. chabaudi* (PCHAS_1323000). Numbers refer to the amino acid position within the PfAP2-HC sequence.

(B, C, D) Amino acid sequence identity matrices of AP2-HC orthologues from eight *Plasmodium* species, comparing the full length protein (panel B), a semi-conserved domain of 172 amino acids (panel C), and the AP2 domain (panel D). Pf, *P. falciparum*. Pv, *P. vivax*. Pk, *P. knowlesi*. Pm, *P. malariae*. Poc, *P. ovale curtisi*. Pb, *P. berghei*. Py, *P. yoelii*. Pc, *P. chabaudi*.

Table S1. Oligonucleotide sequences used for cloning of CRISPR/Cas9 transfection vectors, Related to Figures 1, 2, 4, 5 and 6

Oligonucleotide name	Oligonucleotide sequence 5'→3'	Plasmid name	Cell line name
PCRA_F (Filarsky et al., 2018)	ctggcgtaatagcgaagagg	pD_*gfp-pfap2-hc*, pD_*gfp-pfap2-hc-ΔDBD*	3D7/GFP-PfAP2-HC, 3D7/GFP-PfAP2-HC-ΔDBD
PCRA_R (Filarsky et al., 2018)	cattaatgaatcggccaacg	pD_*gfp-pfap2-hc*, pD_*gfp-pfap2-hc-ΔDBD*	3D7/GFP-PfAP2-HC, 3D7/GFP-PfAP2-HC-ΔDBD
ap2-hc-5'_HR1_F	CGTTGGCCGATTCATTAATGcttatattgtattcagttgattctaac	pD_*gfp-pfap2-hc*	3D7/GFP-PfAP2-HC
ap2-hc-5'_HR1_R	TTCTCCTTTACTCATattttattcttattttgtgtattggttataag	pD_*gfp-pfap2-hc*	3D7/GFP-PfAP2-HC
ap2-hc-5'_GFP_F	AATAAGAATAAAATatgagtaaaggagaagaacttttcac	pD_*gfp-pfap2-hc*	3D7/GFP-PfAP2-HC
ap2-hc-5'_GFP_R	ACTGAATATTCATTtttgtatagttcatccatgccatg	pD_*gfp-pfap2-hc*	3D7/GFP-PfAP2-HC
ap2-hc-5'_HR2_re_F	TGAACTATACAAAaatgaatattcagtttataataagcc	pD_*gfp-pfap2-hc*	3D7/GFP-PfAP2-HC
ap2-hc-5'_HR2_re_R	CCTCTTCGCTATTACGCCAGggtcatctaaatttccattagg	pD_*gfp-pfap2-hc*	3D7/GFP-PfAP2-HC
sgRNA_ap2-hc-5'-1_F	*TATT*gaaacacataacgagcttaa	pH_gC-*ap2-hc-5'*-1	3D7/GFP-PfAP2-HC
sgRNA_ap2-hc-5'-1_R	*AAAC*ttaagctcgttatgtgtttc	pH_gC-*ap2-hc-5'*-1	3D7/GFP-PfAP2-HC
ap2-hc-5'_HR3_F	CGAGTCAGTGAGCGAGGActtatatttgtattcagttgattctaac	pFDon_*ddgfp-pfap2-hc*	3D7/DDGFP-PfAP2-HC
ap2-hc-5'_HR3_R	GTTTCCACCTGCACTCCCATattttattcttattttgtgtattggttataag	pFDon_*ddgfp-pfap2-hc*	3D7/DDGFP-PfAP2-HC
ap2-hc-5'_DD_F	ACACAAAATAAGAATAAAATatggagtgcaggtggaaac	pFDon_*ddgfp-pfap2-hc*	3D7/DDGFP-PfAP2-HC
ap2-hc-5'_DD_R	TTCTTCTCCTTTACTCATACTAGAACCGGTttccagttttagaagctccacac	pFDon_*ddgfp-pfap2-hc*	3D7/DDGFP-PfAP2-HC
ap2-hc-5'_HR4_F	GAGCTTCTAAAACTGGAAACCGGTTCTAGTatgagtaaaggagaagaacttttcac	pFDon_*ddgfp-pfap2-hc*	3D7/DDGFP-PfAP2-HC
ap2-hc-5'_HR4_R	CTTTTCTCTTGTGGATCCGggtcatctaaatttccattagg	pFDon_*ddgfp-pfap2-hc*	3D7/DDGFP-PfAP2-HC
sgRNA_ap2-hc-5'-2_F	*TATT*taacaatatttctgtatcta	pH_gC-*ap2-hc-5'*-2	3D7/DDGFP-PfAP2-HC
sgRNA_ap2-hc-5'-2_R	*AAAC*tagatacagaaatattgtta	pH_gC-*ap2-hc-5'*-2	3D7/DDGFP-PfAP2-HC
ap2-hc-3'_HR1_re_F	CGTTGGCCGATTCATTAATGtaatagagatgaaaatagacaggca	pD_*gfp-pfap2-hc-ΔDBD*	3D7/GFP-PfAP2-HC-ΔDBD
ap2-hc-3'_HR1_re_R	acttttatcataatatactcctttTTAggcttcaaatgatgaaataaccc	pD_*gfp-pfap2-hc-ΔDBD*	3D7/GFP-PfAP2-HC-ΔDBD
ap2-hc-3'_HR2_re_F	ggttatttcatcatttgaagccTAAaaaggagtatattatgataaaagtag	pD_*gfp-pfap2-hc-ΔDBD*	3D7/GFP-PfAP2-HC-ΔDBD
ap2-hc-3'_HR2_re_R	aacaataattcagcttctttttttctctctccattctattgcttttgtc	pD_*gfp-pfap2-hc-ΔDBD*	3D7/GFP-PfAP2-HC-ΔDBD
ap2-hc-3'_HR3_F	acaaaaagcaatagaatggagagagaaaaaagaagctgaattattgtt	pD_*gfp-pfap2-hc-ΔDBD*	3D7/GFP-PfAP2-HC-ΔDBD
ap2-hc-3'_HR3_R	CCTCTTCGCTATTACGCCAGatcatatccatctccatacacaaatg	pD_*gfp-pfap2-hc-ΔDBD*	3D7/GFP-PfAP2-HC-ΔDBD
sgRNA_ap2-hc-3'_F	*TATT*ctagacaaaaggctattgaa	pH_gC-*ap2-hc-3'*	3D7/GFP-PfAP2-HC-ΔDBD
sgRNA_ap2-hc-3'_R	*AAAC*ttcaatagccttttgtctag	pH_gC-*ap2-hc-3'*	3D7/GFP-PfAP2-HC-ΔDBD
ap2-hc-KO_HR1_F	TCAGGGTAGCTGATATCGGATCCcacataacgagcttaatgg	p_gCH-*pfap2-hc*-KO	3D7/PfAP2-HC-KO
ap2-hc-KO_HR1_R	CCTTTTCTCTTGTcattatattcttcaatgtctattac	p_gCH-*pfap2-hc*-KO	3D7/PfAP2-HC-KO
ap2-hc-KO_hDHFR_F	AAGAATATAATGacaagagaaaaggcagaaac	p_gCH-*pfap2-hc*-KO	3D7/PfAP2-HC-KO
ap2-hc-KO_hDHFR_R	CATTACACAAGGACtttaataaatatgttctatatataatgag	p_gCH-*pfap2-hc*-KO	3D7/PfAP2-HC-KO
ap2-hc-KO_HR2_F	CATATTTATTAAAgtccttgtgtaatgaaaatatc	p_gCH-*pfap2-hc*-KO	3D7/PfAP2-HC-KO
ap2-hc-KO_HR2_R	GAGCGAGGAAGCGGAAGCTTgtgtacttggttgatcatatag	p_gCH-*pfap2-hc*-KO	3D7/PfAP2-HC-KO
sgRNA_ap2-hc-KO_F	*TATT*cgttgtactagtaacattgg	p_gCH-*pfap2-hc*-KO	3D7/PfAP2-HC-KO
sgRNA_ap2-hc-KO_R	*AAAC*ccaatgttactagtacaacg	p_gCH-*pfap2-hc*-KO	3D7/PfAP2-HC-KO
F158 (Bui et al., 2019)	CGTTGGCCGATTCATTAATGaaaggatattcagatgatgag	pD_*hp1-mScarlet-glmS*	3D7/GFP-PfAP2-HC/PfHP1-mScarlet-glmS, 3D7/DDGFP-PfAP2-HC/PfHP1-mScarlet-glmS
hp1_HR1_R	CCTTTACTACCTGCGGATCCgctgttctatatcttaatc	pD_*hp1-mScarlet-glmS*	3D7/GFP-PfAP2-HC/PfHP1-mScarlet-glmS,

			3D7/DDGFP-PfAP2-HC/PfHP1-mScarlet-glmS
hp1_mScarlet_F	GATTAAGATATAGAACAGCGgatccgcaggtagtaaagg	pD_*hp1-mScarlet-glmS*	3D7/GFP-PfAP2-HC/PfHP1-mScarlet-glmS, 3D7/DDGFP-PfAP2-HC/PfHP1-mScarlet-glmS
hp1_mScarlet_R	TTGAGAAAATAAGAACAAGAtcatttatataattcatccattcc	pD_*hp1-mScarlet-glmS*	3D7/GFP-PfAP2-HC/PfHP1-mScarlet-glmS, 3D7/DDGFP-PfAP2-HC/PfHP1-mScarlet-glmS
hp1_glmS_F	GAATGGATGAATTATATAAATGAtcttgttcttattttctcaatagg	pD_*hp1-mScarlet-glmS*	3D7/GFP-PfAP2-HC/PfHP1-mScarlet-glmS, 3D7/DDGFP-PfAP2-HC/PfHP1-mScarlet-glmS
hp1_glmS_R	TGTATATTTGCATAATAAAAatttttcttcctcctaagattgtaaaag	pD_*hp1-mScarlet-glmS*	3D7/GFP-PfAP2-HC/PfHP1-mScarlet-glmS, 3D7/DDGFP-PfAP2-HC/PfHP1-mScarlet-glmS
hp1_HR2_F	ATCTTAGGAGGAAGAAAAATttttattatgcaaatatacatatatac	pD_*hp1-mScarlet-glmS*	3D7/GFP-PfAP2-HC/PfHP1-mScarlet-glmS, 3D7/DDGFP-PfAP2-HC/PfHP1-mScarlet-glmS
R163 (Bui et al., 2019)	CCTCTTCGCTATTACGCCAGgaggttaaaattctaaactatatg	pD_*hp1-mScarlet-glmS*	3D7/GFP-PfAP2-HC/PfHP1-mScarlet-glmS, 3D7/DDGFP-PfAP2-HC/PfHP1-mScarlet-glmS

Supplemental Table 1. Oligonucleotide sequences used for cloning of CRISPR/Cas9 transfection vectors. Oligonucleotide names and sequences are shown alongside the plasmid and parasite cell lines they were used to generate. Oligonucleotide sequences used to generate PCR fragments for Gibson assembly reactions (Gibson overhangs) are in upper case. Oligonucleotide sequences required for ligation of annealed double-stranded sgRNA-encoding sequences into the *Bsa*I site of the sgRNA expression cassette are italicized in upper case. A premature STOP codon is highlighted in red font.

Table S2. Primers used for PCRs on gDNA of CRISPR/Cas9-edited gene loci, Related to Figures 1, 2, 4, 5 and 6

Primer name	Primer sequence 5' → 3'	Cell line name
pD_F	accgcctttgagtgagc	
pD_R	cgaaaagtgccacctgacg	
ap2-hc-5'_F	attacttatatttttatttttctcttcaaagaaa	3D7/GFP-PfAP2-HC, 3D7/DDGFP-PfAP2-HC
gfp_R	tccagtgaaaagttcttctcct	3D7/GFP-PfAP2-HC, 3D7/DDGFP-PfAP2-HC
gfp_F	acatggcatggatgaactatacaaa	3D7/GFP-PfAP2-HC, 3D7/DDGFP-PfAP2-HC
ap2-hc-5'_R	acacaaacgctttcactatcttct	3D7/GFP-PfAP2-HC, 3D7/DDGFP-PfAP2-HC
ap2-hc-KO_F	ctaacaatatttctgtatctaaggg	3D7/PfAP2-HC-KO
hDHFR_R	aacgatgcagtttagcgaacc	3D7/PfAP2-HC-KO
hDHFR_F	atgtccaggaggagaaagg	3D7/PfAP2-HC-KO
ap2-hc-KO_R	aggttatttttaactgattatttagagg	3D7/PfAP2-HC-KO
ap2-hc_F	attaaagaattttggagttcctcc	3D7/PfAP2-HC-KO
ap2-hc_R	ctttgtgcattcatcctcagg	3D7/PfAP2-HC-KO
ap2-hc-3'_F	aataaccttcagaagaaatcgcaaa	3D7/GFP-PfAP2-HC-ΔDBD
ap2-hc-3'_R	atcggatatttattctcttgctgttg	3D7/GFP-PfAP2-HC-ΔDBD
hp1_F	gtgtgtgtttaagaaaaaatatg	3D7/GFP-PfAP2-HC/PfHP1-mScarlet-glmS, 3D7/DDGFP-PfAP2-HC/PfHP1-mScarlet-glmS
mScarlet_R	tgtatatttgcataataaaatcatttatataattcatccattccacc	3D7/GFP-PfAP2-HC/PfHP1-mScarlet-glmS, 3D7/DDGFP-PfAP2-HC/PfHP1-mScarlet-glmS
mScarlet_F	gattaagatatagaacagcgggatccgcaggtagtaaagg	3D7/GFP-PfAP2-HC/PfHP1-mScarlet-glmS, 3D7/DDGFP-PfAP2-HC/PfHP1-mScarlet-glmS
hp1_R	catgtagccaaaatatgtg	3D7/GFP-PfAP2-HC/PfHP1-mScarlet-glmS, 3D7/DDGFP-PfAP2-HC/PfHP1-mScarlet-glmS

Supplemental Table 2. Primers used for PCRs on gDNA of CRISPR/Cas9-edited gene loci. Primer names and sequences are shown alongside the parasite cell lines from which gDNA was extracted to carry out PCRs to confirm successful gene editing.

TRANSPARENT METHODS

Parasite culture

P. falciparum 3D7 parasites were cultured as described (Trager and Jenson, 1978) in RPMI Medium 1640 [+] L-Glutamine (Life Technologies) supplemented with 25 mM HEPES, pH 6.72, 100 mM hypoxanthine, 24 mM sodium bicarbonate and 0.5% Albumax II. 2 mM choline chloride was added to the medium to reduce sexual commitment rates (Brancucci et al., 2017). Synchronisation of parasite growth was achieved by repeated sorbitol treatments of ring stage parasites (Lambros and Vanderberg, 1979). Parasite cultures were kept at 37 ºC under a gaseous mixture of 4% CO_2, 3% O_2 and 93% N_2.

Transfection constructs

Transgenic cell lines were generated by CRISPR/Cas9-based genome editing using a set of plasmids recently described (Filarsky et al., 2018). All sgRNA target sequences were identified using CHOPCHOP (Labun et al., 2016; Labun et al., 2019; Montague et al., 2014). 3D7/GFP-PfAP2-HC parasites were created using a two-plasmid approach, consisting of a CRISPR/Cas9 transfection vector pH_gC-*ap2-hc-5'*-1 and the donor plasmid pD_*gfp-pfap2-hc*. The pH_gC-*ap2-hc-5'*-1 plasmid was created by annealing complementary oligonucleotides (sgRNA_ap2-hc-5'-1_F and sgRNA_ap2-hc-5'-1_R) encoding the sgRNA target sequence sgt_ap2-hc-5'-1 (gaaacacataacgagcttaa; positioned at bps +124 to +143 of the *pfap2-hc* coding sequence) and ligating them into the *Bsa*I-digested pH-gC plasmid (Filarsky et al., 2018). The pD_*gfp-pfap2-hc* donor plasmid was produced by Gibson assembly (Gibson et al., 2010; Gibson et al., 2009) of four PCR products encoding (1) the plasmid backbone amplified from pUC19 using primers PCRA_F and PCRA_R (Filarsky et al., 2018), (2) a 5' homology region (HR) spanning 575 bp of the *pfap2-hc* upstream region amplified from 3D7 gDNA using primers ap2-hc-5'_HR1_F and ap2-hc-5'_HR1_R, (3) the *gfp* coding sequence amplified from plasmid pD_*ap2g-gfp-dd-glmS* (Filarsky et al., 2018) using primers ap2-hc-5'_GFP_F and ap2-hc-5'_GFP_R, and (4) a 745 bp 3' HR corresponding to the *pfap2-hc* coding region +3 to +748. Fragment 4 was ordered as synthetic sequence (GenScript) with the first 274 bp recodonised and was amplified from plasmid pUC57-re-*ap2-hc*-1 using primers ap2-hc-5'_HR2_re_F and ap2-hc-5'_HR2_re_R.
The 3D7/DDGFP-PfAP2-HC parasite line was generated using plasmids pH_gC-*ap2-hc-5'*-2 and pFDon_*ddgfp-pfap2-hc*. To generate pH_gC-*ap2-hc-5'*-2, complementary oligonucleotides (sgRNA_ap2-hc-5'-2_F and sgRNA_ap2-hc-5'-2_R) encoding the sgRNA target sequence sgt_ap2-hc-5'-2 (taacaatatttctgtatcta; positioned at bps +36 to +55 of the *pfap2-hc* coding sequence) were annealed and ligated into the *Bsa*I-digested pH-gC plasmid (Filarsky et al., 2018). pFDon_*ddgfp-pfap2-hc* donor plasmid was created by Gibson assembly of four fragments: (1) the pFDon plasmid (Filarsky et al., 2018) digested with *Hind*III and *Eco*RI, (2, 3) the 5' HR and the *gfp*-3'HR were amplified from plasmid pD_*gfp-pfap2-hc* (described above) with primers ap2-hc-5'_HR3_F and ap2-hc-5'_HR3_R, and ap2-hc-5'_HR4_F and ap2-hc-5'_HR4_R, respectively. The final fragment 4 encoding the FKBP destabilizing domain (*dd*) sequence (plus C-terminal TGSS linker) was amplified from pD_*ap2g-gfp-dd-glmS* (Filarsky et al., 2018) using primers ap2-hc-5'_DD_F and ap2-hc-5'_DD_R.
Parasite line 3D7/GFP-PfAP2-HC-ΔDBD was created by CRISPR/Cas9 editing of 3D7/GFP-PfAP2-HC parasites using plasmids pH_gC-*ap2-hc-3'* and pD_*gfp-pfap2-hc-*Δ*DBD*. The sgRNA-encoding oligonucleotides sgRNA_ap2-hc-3'_F and sgRNA_ap2-hc-3'_R were annealed and ligated into the *Bsa*I-digested pH-gC plasmid (Filarsky et al., 2018), as above, to create pH_gC-*ap2-hc-3'*. The sgRNA target sequence sgt_ap2-hc-3' (ctagacaaaaggctattgaa) is positioned at bps +4070 to +4089 of the *pfap2-hc* coding sequence. To create pD_*gfp-pfap2-hc-*Δ*DBD*, a synthetic DNA sequence (GenScript), corresponding to the *pfap2-hc* coding sequence +3528 to +4125 with the intron removed and the sequence +3954 to +4125 recodonised (plasmid pUC57-re-*ap2-hc*-2). To introduce a STOP codon prior to the sequence encoding the AP2 DBD two overlapping PCR fragments (1, 2) were amplified from pUC57-re-*ap2-hc*-2 using primers ap2-hc-3'_HR1_re_F and ap2-hc-3'_HR1_re_R, and ap2-hc-3'_HR2_re_F and ap2-hc-3'_HR2_re_R, respectively. The ap2-hc-3'_HR1_re_R and ap2-hc-3'_HR2_re_F primers introduce a TAA STOP codon at amino acid position 1319 (R1319*). Fragments (1, 2) were assembled together with fragment 3 representing the plasmid backbone amplified from pUC19 using primers PCRA_F and PCRA_R (Filarsky et al., 2018), and fragment 4 representing the 3' HR beginning at nucleotide +4088 of the *pfap2-hc* coding sequence and ending 852 bp downstream of the native STOP codon (76 bp into the neighbouring gene PF3D7_1456100) and amplified from 3D7 gDNA using primers ap2-hc-3'_HR3_F and ap2-hc-3'_HR3_R.
3D7/GFP-PfAP2-HC/PfHP1-mScarlet-glmS and 3D7/DDGFP-PfAP2-HC/PfHP1-mScarlet-glmS parasite lines were generated by editing the endogenous *pfhp1* locus in parasites lines 3D7/GFP-PfAP2-HC and 3D7/DDGFP-PfAP2-HC, respectively. The recently published CRISPR/Cas9 plasmid

pBF-gC-guide250 (Bui et al., 2019) was used in combination with the donor plasmid pD_*hp1-mScarlet-glmS*. The donor construct was created by joining five fragments in a Gibson assembly consisting of (1, 2) previously described 5' and 3' HRs amplified from plasmid pD-PfHP1-KO (Bui et al., 2019), using primers F158 and hp1_HR1_R, and hp1_HR2_F and R163, respectively. Fragment 3, consisting of a *P. falciparum* codon-optimised *mScarlet* sequence with an N-terminal GSAG linker, was amplified from the plasmid pD_*ap2-g-mScarlet* (Brancucci et al., manuscript in preparation) using primers hp1_mScarlet_F and hp1_mScarlet_R. The *glmS* sequence (fragment 4) was amplified from plasmid pL6-3HA_glmS-246 (kind gift from Dave Richard) using primers hp1_glmS_F and hp1_glmS_R, and finally, the plasmid backbone (fragment 5), was amplified from pUC19 with primers PCRA_F and PCRA_R (Filarsky et al., 2018).
The 3D7/PfAP2-HC-KO cell line was created using a single plasmid CRISPR/Cas9 approach. The mother plasmid p_gC (Filarsky et al., 2018) formed the backbone to create p_gCH-*pfap2-hc*-KO. p_gC was digested with *Bam*HI and *Hind*III and used in a Gibson assembly with (1) a 5' HR spanning bps +128 to +533 of the *pfap2-hc* coding sequence, amplified from 3D7 gDNA with primers ap2-hc-KO_HR1_F and ap2-hc-KO_HR1_R, (2) a *hdhfr* expression cassette amplified from plasmid p_gCH-*gdv1*-asKO (Filarsky et al., 2018) (primers ap2-hc-KO_hDHFR_F and ap2-hc-KO_hDHFR_R), and (3) a 3' HR spanning bps +3042 to +3460 of the *pfap2-hc* coding sequence, amplified from 3D7 gDNA using primers ap2-hc-KO_HR2_F and ap2-hc-KO_HR2_R. The resulting plasmid, p_gCH-*pfap2-hc*-KO-pre, was digested with *Bsa*I and the sgRNA-encoding sequence sgt_ap2-hc-KO (cgttgtactagtaacattgg; position +1724 to +1743 of the *pfap2-hc* coding sequence, negative strand) was created by annealing the complementary oligonucleotides sgRNA_ap2-hc-KO_F and sgRNA_ap2-hc-KO_R, and ligated into the *Bsa*I site creating the final p_gCH-*pfap2-hc*-KO plasmid.
Oligonucleotide sequences used in cloning are provided in Table S1.

Transfection and transgenic cell lines
P. falciparum parasite transfections were carried out as described (Filarsky et al., 2018; Voss et al., 2006). A total of 100 µg plasmid DNA (two-plasmid CRISPR/Cas9 approach: 50 µg of each plasmid; single-plasmid CRISPR/Cas9 approach: 100 µg plasmid) was transfected into 3D7/WT or previously engineered parasites and the cultures allowed to recover for 24 hours by growth in drug-free culture medium. Selection of transgenics was then initiated by the addition of 4 nM WR99210 for a total of six days for pH-derived plasmids, or continuously for plasmid p_gCH-*pfap2-hc*-KO. Parasites transfected with the pBF-gC-guide250 construct were selected with 2.5 µg/mL blasticidin-S-hydrochloride for a total of ten days. 3D7/DDGFP-PfAP2-HC parasites were cultured in the presence of 700 nM Shield-1 (+Shield-1) unless otherwise stated. Induction of PfHP1 depletion in parasite lines 3D7/GFP-PfAP2-HC/PfHP1-mScarlet-glmS and 3D7/DDGFP-PfAP2-HC/PfHP1-mScarlet-glmS was achieved by the addition of 2.5 mM glucosamine (GlcN, Sigma #G4875). Limiting dilution cloning was carried out on parasites lines 3D7/GFP-PfAP2-HC, 3D7/DDGFP-PfAP2-HC and 3D7/GFP-PfAP2-HC-ΔDBD as described (Thomas et al., 2016). Successful gene editing was confirmed by PCR on gDNA using primers listed in Table S2.

Fluorescence microscopy
Live cell fluorescence imaging was performed as previously described (Witmer et al., 2012) with the minor modification of nuclear staining with Hoechst (Merck) instead of DAPI at a final concentration of 5 µg/ml. IFAs were carried out on methanol-fixed cells using primary antibodies mouse mAb α-GFP (Roche Diagnostics #11814460001) (1:100) and rabbit α-PfHP1 (Brancucci et al., 2014) (1:100). Secondary antibodies Alexa Fluor 488-conjugated α-mouse IgG (Invitrogen #A11001) and Alexa Fluor 568-conjugated α-rabbit IgG (Invitrogen #A11011) were used, each at 1:250 dilution. Nuclei were stained during slide preparation with Vectashield containing DAPI (Vector Laboratories). Images were acquired on a Leica DM 5000B microscope with a Leica DFC 345 FX camera using the Leica application suite (LAS) software. Image processing was carried out using Fiji (Schindelin et al., 2012). For each experiment, all images were acquired and processed with identical settings.

Western blot
Whole parasite protein extracts were prepared by first releasing parasites from the iRBC by saponin lysis (0.15% in PBS) followed by suspension of the parasite pellet in UREA/SDS lysis buffer [(8 M Urea, 5% SDS, 50 mM Bis-Tris, 2 mM EDTA, 25 mM HCl, pH 6.5, 1 mM DTT, 1x protease inhibitor (Roche)] and separated on a NuPage 3-8% Tris-Acetate gel (Novex) using NuPage MES SDS Running Buffer (Novex). Proteins were detected with primary antibodies mouse mAb α-GFP (Roche Diagnostics #11814460001) (1:1000), rabbit α-PfHP1 (Brancucci et al., 2014) (1:5000), and mouse mAb α-GAPDH (Daubenberger et al., 2003), (1:10000), and secondary antibodies α-mouse IgG (H&L)-HRP (GE healthcare #NXA931) (1:5000) and α-rabbit IgG (H&L)-HRP (GE Healthcare #NA934)

(1:5000). Chemiluminescence signal was detected using KPL LumiGLO Reserve Chemiluminescent Substrate Kit (SeraCare #5430-0049).

Chromatin immunoprecipitations

Parasite cultures were synchronised to obtain an eight-hour growth window and harvested at peak PfAP2-HC expression at 36-44 hpi (Bartfai et al., 2010) from a 30 ml culture at 5% haematocrit and 4-5% parasitemia. Parasites were crosslinked with 1% formaldehyde for 10 min at 37 °C before quenching with 0.125 M glycine. The RBC membrane was lysed with 0.15% saponin and cytoplasmic lysis buffer [(CLB: 20 mM Hepes, 10 mM KCl, 1 mM EDTA, 1 mM EGTA, 0.65% NP-40, 1 mM DTT, 1x protease inhibitor (Roche)] was added to the parasite pellet to isolate nuclei. Nuclei were then snap-frozen in liquid nitrogen in CLB supplemented with 50% glycerol and stored at -80 °C. Chromatin isolation, shearing and immunoprecipitation was performed according to previously published protocols (Filarsky et al., 2018). To prepare chromatin, frozen nuclei were thawed, pelleted and resuspended in 150 µl sonication buffer [(50 mM Tris pH 8, 1% SDS, 10 mM EDTA, 1x protease inhibitor (Roche)], and were sonicated for 20 cycles of 30 sec ON/30 sec OFF (setting high, BioruptorTM Next Gen, Diagenode) to shear DNA to fragments of 100-600 bps. Fragment size was confirmed by de-crosslinking a 15 µl aliquot and visualising the purified DNA on a 2% agarose gel. ChIPs were performed by combining sonicated chromatin (500 ng DNA content) with either 1 µg mouse mAb α-GFP (Roche Diagnostics #11814460001) or 1 µg rabbit α-PfHP1 (Brancucci et al., 2014) in incubation buffer [(5% Triton-X-100, 750 mM NaCl, 5 mM EDTA, 2.5 mM EGTA, 100 mM Hepes pH 7.4, 0.2% bovine serum albumin, 1x protease inhibitor (Roche)] containing 10 µl protA and 10 µl protG Dynabeads (Life Technologies, #10008D and #10009D, respectively) in a total reaction volume of 300 µl. ChIP samples were incubated overnight at 4 °C with rotation. Beads were washed for 5 min at 4 °C, with rotation, with 400 µl wash buffers as follows: 2x wash buffer 1 (0.1% SDS, 0.1% DOC, 1% Triton-X100, 150 mM NaCl, 1 mM EDTA, 0.5 mM EGTA, 20 mM Hepes pH 7.4), 1x wash buffer 2 (0.1% SDS, 0.1% DOC, 1% Triton-X100, 500 mM NaCl, 1 mM EDTA, 0.5 mM EGTA, 20 mM Hepes pH 7.4), 1x wash buffer 3 (250 mM LiCl, 0.5% DOC, 0.5% NP-40, 1 mM EDTA, 0.5 mM EGTA, 20 mM Hepes pH 7.4), 2x wash buffer 4 (1 mM EDTA, 0.5 mM EGTA, 20 mM Hepes pH 7.4). Immunoprecipitated chromatin was eluted from the beads by shaking at room temperature for 20 min in 200 µl elution buffer (1% SDS, 0.1 M $NaHCO_3$) and de-crosslinked at 45 °C overnight in 1% SDS, 0.1 M $NaHCO_3$ and 1 M NaCl. Simultaneously, 30 µl of sonicated input chromatin was de-crosslinked under the same conditions. DNA was purified with QIAquick MinElute PCR columns (Qiagen). For each ChIP-seq experiment, twenty separate α-GFP ChIPs or four separate α-PfHP1 ChIPs were combined, with the exception of 3D7/GFP-PfAP2-HC/PfHP1-mScarlet-glmS α-PfHP1 ChIP-seq for which eight separate ChIPs were combined.

High throughput sequencing and data analysis

The obtained ChIPed DNA fragments were used to generate Illumina sequencing libraries according to Filarsky et al. (Filarsky et al., 2018). In brief, 1 ng of α-PfHP1 ChIP, α-GFP ChIP, or input DNA were end-repaired with T4 DNA polymerase (NEB, M0203L), Klenow DNA polymerase (NEB, M0210L), and T4 Polynucleotide Kinase (NEB, M0201L). The 3'ends of end-repaired DNA were extended with an A-overhang with 3' to 5' exonuclease-deficient Klenow DNA polymerase (NEB, M0212L). The resulting fragments were ligated to Nextflex 6bp adaptors (Bio Scientific, #514122) with the use of T4 DNA ligase (Promega, M1804). The libraries were amplified using an AT-rich optimized KAPA protocol using KAPA HiFi HotStart ready mix (KAPA Biosystems, KM2602), NextFlex primer mix (Bio Scientific, #514122) with the following PCR program: 98°C for 2 min; four cycles of 98°C for 20 sec, 62°C for 3 min; 62°C for 5 min. The fragments originating from mono-nucleosomes + 125 bp NextFlex adapter were selected using 2% E-Gel Size Select agarose gels (Invitrogen, #G6610-02) and amplified by PCR for nine cycles using the above conditions. Libraries were purified and adapter dimers removed with Agencourt AMPure XP beads purification using a 1:1 library:beads ratio (Beckman Coulter, #A63880). ChIP-seq libraries were sequenced on the Illumina NextSeq 500 system with a 20% phiX spike-in (Illumina, FC-110-3001) to generate 75 bp single-end reads (NextSeq 500/550 High Output v2 kit). The quality of the resulting reads were checked with FastQC (V0.11.8) and the reads were mapped against the *P. falciparum* 3D7 reference genome from PlasmoDB v26 (www.plasmodb.org) using BWA samse (v0.7.17-r1188) (Andrews, 2010; Li and Durbin, 2009). Mapped reads originating from the mitochondrial and apicoplast genome, multi-mapping reads, and reads having a mapping quality below 15 were removed (SAMtools v1.9) (Li et al., 2009) leaving between 4.8 and 25.4 million reads (note that replicate 2 of 3D7/GFP-PfAP2-HC/PfHP1-mScarlet-glmS cultured in presence of GlcN (Figure 5D) is based on 2.0 million reads). Before visualising the ChIP-seq data in the UCSC Genome browser (Figures 1E-G, 2D, 4C, 5D) or Signalmap (version 2.0.0.5) (Figure 1C), the libraries were normalised to the total amount of reads, reads per million, with bedtools genomeCoverageBed

(v2.27.1) and the enrichment over the input sample was calculated by dividing ChIP sample with input sample read counts, which subsequently was log2 transformed (one pseudo count was added to avoid division by zero) (Kent et al., 2002; Quinlan and Hall, 2010). Within the UCSC genome browser, tracks were smoothened (8) and the windowing function was set as 'mean'. To enable the visualisation of all chromosomes together Signalmap (version 2.0.0.5) was used. The average log2 Chip-over-input value was calculated in sequential 1kb windows to smoothen and compress the data set. PfHP1 values are visualised on the positive scale shifted up by 2 and PfAP2-HC (GFP) values are visualised in the negative scale shifted up by 1. The enrichment tracks were shifted to show the complete tracks. To show the genome-wide colocalization of PfHP1 and PfAP2-HC occupancy and comparison between cell lines the average log2 Chip-over-input ratios at coding genes were calculated using bedtools genomeCoverageBed (v2.27.1) (Quinlan and Hall, 2010) (Dataset S1) and visualised with Excel 2016. Genes with PfHP1 log2 ChIP-over-input ratios of greater than or equal to zero were classified as heterochromatic genes. The position of putative AP2-HC binding sites (i.e. CACACA motifs) has been defined using the position weight matrix of the CACACA motif as described by Campbell et al. (Campbell et al., 2010) and searching the *P falciparum* genome for matching sequences (fdr<0.05) with the use of the gimme scan tool of GimmeMotifs (van Heeringen and Veenstra, 2011).

Flow cytometry

Synchronous 3D7/DDGFP-PfAP2-HC and 3D7/WT parasites were split at 0-8 hpi to 0.1% parasitaemia and cultured either in the presence of 700 nM Shield-1 (+ Shield-1) or absence of Shield-1 (- Shield-1) during the duration of the multiplication assay. Synchronous 3D7/PfAP2-HC-KO parasites at 0-8 hpi were diluted to 0.1% parasiteamia. After 24 hours (24-32 hpi) parasite DNA was stained with SYBR Green DNA stain (1: 10,000) (Invitrogen #S7563) for 30 min at 37 °C and the fluorescence intensity was measured using a MACS Quant Analyzer 10 (at least 200,000 RBCs were measured per sample) to determine the parasitaemia (day 1). Measurements were repeated on day 3 and day 5 at 24-32 hpi. Data were analysed using the FlowJo_v10.6.1 software. Gating was performed to remove debris smaller than cell size, to include only single measurement events and to separate uninfected from infected RBCs based on the SYBR Green intensity of an uninfected RBC control sample (the gates for 'cells', 'singlets' and 'parasites', respectively, are shown in Figure S2).

Quantification of sexual conversion rates

3D7/DDGFP-PfAP2-HC and 3D7/WT parasites were synchronised with sorbitol to a 6-hour time window and again in the next generation after RBC invasion at 0-6 hpi, after which each culture was split and one half was maintained in the presence of Shield-1 (+ Shield-1) and the other half was cultured in the absence of Shield-1 (- Shield-1). Eighteen hours later (18-24 hpi), cultures were split again (1-2% parasitaemia, 2.5% haematocrit) and grown in either minimal fatty acid (mFA) medium [RPMI Medium 1640 [+] L-Glutamine (Life Technologies) supplemented with 25 mM HEPES, pH 6.72, 100 mM hypoxanthine, 24 mM sodium bicarbonate, 0.39% fatty acid-free BSA (Sigma #A6003), 30 µM oleic acid and 30 µM palmitic acid], which induces sexual commitment, or mFA medium supplemented with 2 mM choline chloride (mFA+CC), which inhibits sexual commitment (Brancucci et al., 2017). After 24 hours (42-48 hpi), mFA or mFA+CC medium was replaced with the standard Albumax medium used throughout this study (see above). After invasion into new RBCs, 50 mM N-acetylglucosamine (GlcNAc) was added to the cultures at 24-30 hpi (day 1 of gametocytogenesis) to prevent asexual parasite multiplication (Fivelman et al., 2007; Ponnudurai et al., 1986). The resulting gametocyte cultures were maintained in the presence of GlcNAc for a further 3 days. Parasitaemia on day 1 of gametocytogenesis (mixture of asexuals and sexual ring stage parasites) and gametocytemia on day 4 of gametocytogenesis were counted and sexual conversion rates were calculated (gametocytaemia [%] / parasitaemia [%] * 100 = sexual conversion rate [%]).

Microarray Experiments and Data Analysis

3D7/DDGFP-PfAP2-HC parasites, continuously cultured in the presence of Shield-1, were synchronised with sorbitol to obtain an eight-hour growth window (16-24 hpi) and again in the next generation after RBC invasion at 0-8 hpi. The culture was then split at 8-16 hpi and one half was maintained in the presence of Shield-1 (+Shield-1) and the other half was cultured in the absence of Shield-1 (-Shield-1) to achieve DDGFP-PfAP2-HC depletion. The parasites proceeded through the IDC and were harvested for total RNA extraction in the subsequent generation at the following time points: TP1 (8-16 hpi), TP2 (16-24 hpi), TP3 (24-32 hpi), TP4 (32-40 hpi) and TP5 (40-48 hpi). RNA isolation and cDNA synthesis were performed as previously described (Bozdech et al., 2003). Cy5-labelled sample cDNAs were hybridised against a Cy3-labelled cDNA reference pool prepared from 3D7 wild-type parasites (Brancucci et al., 2014). Equal amounts of Cy5- and Cy3-labelled samples

were hybridised on a *P. falciparum* 8×15K Agilent gene expression microarray (GEO platform ID GPL15130) (Painter et al., 2013) for 16 hours at 65°C in an Agilent hybridisation oven (G2545A). Slides were scanned using the GenePix scanner 4000B and GenePix pro 6.0 software (Molecular Devices). The raw microarray data representing relative steady state mRNA abundance ratios between each test sample and the reference pool (Cy5/Cy3 log2 ratios) were subjected to lowess normalization and background filtering as implemented by the Acuity 4.0 program (Molecular Devices). Flagged features and features with either Cy3 or Cy5 intensities lower than two-fold the background were removed. Log2 ratios for multiple probes per gene were averaged and genes recognized by non-uniquely mapping probes were removed from the dataset. Transcripts showing expression values in at least four of the five samples harvested for each time course were included for downstream analysis to identify genes differentially expressed [mean fold change cut-off > 2; p-value cut-off 0.01 (paired two-tailed Student's t-test)] between control (+Shield-1) and DDGFP-AP2-HC-depleted (-Shield-1) parasites. The processed microarray dataset is listed in Dataset S2.

Induction of gametocytogenesis by conditional depletion of PfHP1

3D7/DDGFP-PfAP2-HC/PfHP1-mScarlet-glmS parasites were synchronised to obtain an eight-hour growth window and re-synchronised in the following cycle at 0-8 hpi (generation 1). The culture was split into two populations, one grown in the presence of Shield-1 and one in the absence of Shield-1. Both parasite populations were synchronised again at 0-8 hpi in the following cycle (generation 2) and 2.5 mM glucosamine (GlcN, Sigma #G4875) was added to induce PfHP1 depletion (+Shield-1/+GlcN and –Shield-1/+GlcN). Parasites progressed through generation 2 and in generation 3, GlcN was removed from both populations and parasites were cultured on serum medium (0.5% Albumax replaced with 10% human serum) containing 50 mM N-acetylglucosamine (GlcNAc) to prevent asexual parasite multiplication (Fivelman et al., 2007; Ponnudurai et al., 1986). Live cell fluorescence imaging was performed in stage II and stage V gametocytes to observe PfHP1-mScarlet signals between +Shield-1 (DDGFP-AP2-HC-expressing) and -Shield-1 (DDGFP-AP2-HC-depleted) parasites. The experimental design is depicted schematically in Figure 6B.

Multiple sequence alignment of AP2-HC orthologues

Orthologues of PfAP2-HC (PF3D7_1456000) were identified on www.plasmodb.org (Aurrecoechea et al., 2009) from *P. vivax* (PVX_117665), *P. knowlesi* (PKNH_1225800), *P. malariae* (PmUG01_12060900), *P. ovale curtisi* (PocGH01_12058800), *P. berghei* (PBANKA_1319700), *P. yoelii* (PY17X_1323500) and *P. chabaudi* (PCHAS_1323000) and their full length amino acid sequences were aligned using Clustal X2.1 (Larkin et al., 2007) multiple sequence alignment on default settings. A tree was generated using Clustal X2.1 (Larkin et al., 2007) on default settings and the resulting identity matrix was tabulated. The AP2 domains of each orthologue were aligned separately and an identity matrix generated. A semi-conserved domain (spanning amino acids 995-1126 of PfAP2-HC) was identified, aligned separately and an identity matrix generated.

SUPPLEMENTAL REFERENCES

Andrews, S., (2010). FastQC: A quality control tool for high throughput sequence data. Available online at: https://www.bioinformatics.babraham.ac.uk/projects/fastqc.

Bozdech, Z., Llinas, M., Pulliam, B.L., Wong, E.D., Zhu, J., and DeRisi, J.L. (2003). The transcriptome of the intraerythrocytic developmental cycle of Plasmodium falciparum. PLoS Biol. 1(1), E5.

Brancucci, N.M.B., Gerdt, J.P., Wang, C., De Niz, M., Philip, N., Adapa, S.R., Zhang, M., Hitz, E., Niederwieser, I., Boltryk, S.D., et al. (2017). Lysophosphatidylcholine Regulates Sexual Stage Differentiation in the Human Malaria Parasite Plasmodium falciparum. Cell. 171(7), 1532-1544 e1515.

Bui, H.T.N., Niederwieser, I., Bird, M.J., Dai, W., Brancucci, N.M.B., Moes, S., Jenoe, P., Lucet, I.S., Doerig, C., and Voss, T.S. (2019). Mapping and functional analysis of heterochromatin protein 1 phosphorylation in the malaria parasite Plasmodium falciparum. Scientific Reports. 9(1), 16720.

Daubenberger, C.A., Tisdale, E.J., Curcic, M., Diaz, D., Silvie, O., Mazier, D., Eling, W., Bohrmann, B., Matile, H., and Pluschke, G. (2003). The N'-terminal domain of glyceraldehyde-3-phosphate dehydrogenase of the apicomplexan Plasmodium falciparum mediates GTPase Rab2-dependent recruitment to membranes. Biol. Chem. 384(8), 1227-1237.

Gibson, D.G., Smith, H.O., Hutchison, C.A., 3rd, Venter, J.C., and Merryman, C. (2010). Chemical synthesis of the mouse mitochondrial genome. Nat. Methods. 7(11), 901-903.

Gibson, D.G., Young, L., Chuang, R.Y., Venter, J.C., Hutchison, C.A., III, and Smith, H.O. (2009). Enzymatic assembly of DNA molecules up to several hundred kilobases. Nat. Methods. 6(5), 343-345.

Kent, W.J., Sugnet, C.W., Furey, T.S., Roskin, K.M., Pringle, T.H., Zahler, A.M., and Haussler, D. (2002). The human genome browser at UCSC. Genome Res. 12(6), 996-1006.

Labun, K., Montague, T.G., Gagnon, J.A., Thyme, S.B., and Valen, E. (2016). CHOPCHOP v2: a web tool for the next generation of CRISPR genome engineering. Nucleic Acids Res. 44(W1), W272-W276.

Labun, K., Montague, T.G., Krause, M., Torres Cleuren, Y.N., Tjeldnes, H., and Valen, E. (2019). CHOPCHOP v3: expanding the CRISPR web toolbox beyond genome editing. Nucleic Acids Res. 47(W1), W171-W174.

Lambros, C., and Vanderberg, J.P. (1979). Synchronization of Plasmodium falciparum erythrocytic stages in culture. J. Parasitol. 65(3), 418-420.

Larkin, M.A., Blackshields, G., Brown, N.P., Chenna, R., McGettigan, P.A., McWilliam, H., Valentin, F., Wallace, I.M., Wilm, A., Lopez, R., et al. (2007). Clustal W and Clustal X version 2.0. Bioinformatics. 23(21), 2947-2948.

Li, H., and Durbin, R. (2009). Fast and accurate short read alignment with Burrows-Wheeler transform. Bioinformatics. 25(14), 1754-1760.

Li, H., Handsaker, B., Wysoker, A., Fennell, T., Ruan, J., Homer, N., Marth, G., Abecasis, G., Durbin, R., and Genome Project Data Processing, S. (2009). The Sequence Alignment/Map format and SAMtools. Bioinformatics. 25(16), 2078-2079.

Montague, T.G., Cruz, J.M., Gagnon, J.A., Church, G.M., and Valen, E. (2014). CHOPCHOP: a CRISPR/Cas9 and TALEN web tool for genome editing. Nucleic Acids Res. 42(Web Server issue), W401-W407.

Quinlan, A.R., and Hall, I.M. (2010). BEDTools: a flexible suite of utilities for comparing genomic features. Bioinformatics. 26(6), 841-842.

Schindelin, J., Arganda-Carreras, I., Frise, E., Kaynig, V., Longair, M., Pietzsch, T., Preibisch, S., Rueden, C., Saalfeld, S., Schmid, B., et al. (2012). Fiji: an open-source platform for biological-image analysis. Nat. Methods. 9(7), 676-682.

Thomas, J.A., Collins, C.R., Das, S., Hackett, F., Graindorge, A., Bell, D., Deu, E., and Blackman, M.J. (2016). Development and Application of a Simple Plaque Assay for the Human Malaria Parasite Plasmodium falciparum. PLoS. ONE. 11(6), e0157873.

Trager, W., and Jenson, J.B. (1978). Cultivation of malarial parasites. Nature. 273(5664), 621-622.

van Heeringen, S.J., and Veenstra, G.J. (2011). GimmeMotifs: a de novo motif prediction pipeline for ChIP-sequencing experiments. Bioinformatics. 27(2), 270-271.

Voss, T.S., Healer, J., Marty, A.J., Duffy, M.F., Thompson, J.K., Beeson, J.G., Reeder, J.C., Crabb, B.S., and Cowman, A.F. (2006). A var gene promoter controls allelic exclusion of virulence genes in Plasmodium falciparum malaria. Nature. 439(7079), 1004-1008.

Witmer, K., Schmid, C.D., Brancucci, N.M., Luah, Y.H., Preiser, P.R., Bozdech, Z., and Voss, T.S. (2012). Analysis of subtelomeric virulence gene families in Plasmodium falciparum by comparative transcriptional profiling. Mol. Microbiol. 84(2), 243-259.